ChemPubSoc Europe
DOI: 10.1002/ejic.201501406
EurJIC European Journal of Inorganic Chemistry
Full Paper

Non-Heme Iron Complexes

# Mimicry of the 2-His-1-Carboxylate Facial Triad Using Bulky N,N,O-Ligands: Non-Heme Iron Complexes Featuring a Single Facial Ligand and Easily Exchangeable Co-Ligands

Emma Folkertsma,[a] Esther F. de Waard,[a] Gerda Korpershoek,[a] Arnoldus J. van Schaik,[a] Naiara Solozabal Mirón,[a] Mandy Borrmann,[a] Sjoerd Nijsse,[a] Marcel A. H. Moelands,[a] Martin Lutz,[b] Matthias Otte,[a] Marc-Etienne Moret,,[a] and Robertus J. M. Klein Gebbink*[a]

**Abstract:** Mononuclear iron(II) complexes with facially coordinating N,N,O-ligands were synthesized as accurate structural mimics of the 2-His-1-carboxylate facial triad found in mononuclear non-heme iron enzymes. Mimicking of the facial triad is achieved by designing sterically demanding ligands providing two histidine-like benzimidazole moieties and a coordinating carboxylate or ester moiety. The new methyl-substituted analogue of the bis(benzimidazolyl)propionate ligand, BMB$^{Me}$IP and its ester analogue, BMB$^{Me}$IP$^{nPr}$ are designed to prevent the formation of previously reported coordinatively saturated $FeL_2$ type complexes. The crystal structure of [Fe(BMB$^{Me}$IP$^{nPr}$)(OTf)$_2$] shows a facial N,N,O-coordination that is very similar to the structure of the enzyme active sites. Both [Fe(BMB$^{Me}$IP$^{nPr}$)(OTf)$_2$] and [Fe(BMB$^{Me}$IP)(OTf)(MeCN)$_n$] catalyze the epoxidation of olefins using $H_2O_2$, reaching turnover numbers up to 5.8 per iron. These results represent the first examples of iron complexes bearing a single facial and rigid N,N,O-coordinating ligand and three readily available coordination sites showing catalytic activity in oxidation reactions.

## Introduction

Iron-based metalloenzymes, which are commonly found in nature, are well known for their ability to catalyze a wide range of reactions in which molecular oxygen is activated.[1] In the superfamily of mononuclear non-heme iron oxygenases a common structural motif, in which the active site contains an iron center that is facially coordinated by two histidines and one carboxylato group, is established.[2,3] We have a particular interest in this so-called 2-His-1-carboxylate facial triad because of its unique reactivity scope including selective *cis*-dihydroxylation, oxidative ring cleavage, epoxidation of alkenes, and oxidative C–N bond formation and ring closure.[4,5] To date, the activity of non-heme iron enzymes is mimicked most efficiently by iron complexes derived from $N_4$-type ligands such as BPMEN, $Me_2$PyTACN, PDP, and TPA (Figure 1).[1,6–17] Highly active and selective catalysts for the epoxidation of olefins with turnover numbers over 120 and high stereoselectivity (97 % *ee*)[18] have been described.[10,19–25] Most of these complexes are structurally distinct from the typical non-heme enzyme active site in the sense that these lack a carboxylate, or in general an O-donor moiety and that the N-donors often stem from a pyridine ring instead of imidazole rings.

A number of efforts on the use of mixed N,O-ligands in mimicry studies of the facial triad have been reported. The main challenge is to isolate a mono-ligand complex that is catalytically active in oxidation catalysis. The mono-ligand iron(II) complex [Fe(L1)(X)] (X = OTf or Cl), featuring a bidentate carboxylate within a facial ligand setting, closely resembles the facial triad coordination sphere, as reported by Que et al. (Figure 1).[19] This complex is active in the epoxidation as well as in the *cis*-dihydroxylation of olefins, although catalytic turnover was not achieved. Studies by Rutledge et al. focused on the use of mixed N,O-ligands based on a central pyridine donor (H2-R; Figure 1). The use of in situ generated complexes bearing H2-R ligands in the oxidation of alkenes resulted in low activity (up to 0.2 turnovers).[26,27] Our group recently reported the first example of an oxidation catalyst with a single chiral facial N,N,O-ligand: the [Fe(PyProMe)$Cl_2$] complex (Figure 1).[28] The use of this and related iron complexes resulted in good turnover numbers (up to 50) in the epoxidation of olefins, but no significant enantioselectivity was obtained.[28,29] However, the structure of this complex is very flexible and the chiral pyridinyl prolinate ligand easily isomerizes between facial and meridional coordination modes. Many other studies resulted in the isolation of bis-ligand complexes; for example, Burzlaff et al. found that the bis(pyrazolyl)acetate ligand (bdmpzaH) affords $FeL_2$ type and

[a] *Organic Chemistry and Catalysis, Debye Institute for Nanomaterials Science, Faculty of Science, Utrecht University, Universiteitsweg 99, 3584 CG Utrecht, The Netherlands*
*E-mail: r.j.m.kleingebbink@uu.nl*
*http://www.uu.nl/en/research/organic-chemistry-catalysis*
[b] *Crystal and Structural Chemistry, Bijvoet Center for Biomolecular Research, Faculty of Science, Utrecht University, Padualaan 8, 3584 CH Utrecht, The Netherlands*
*Supporting information and ORCID(s) from the author(s) for this article are available on the WWW under http://dx.doi.org/10.1002/ejic.201501406.*

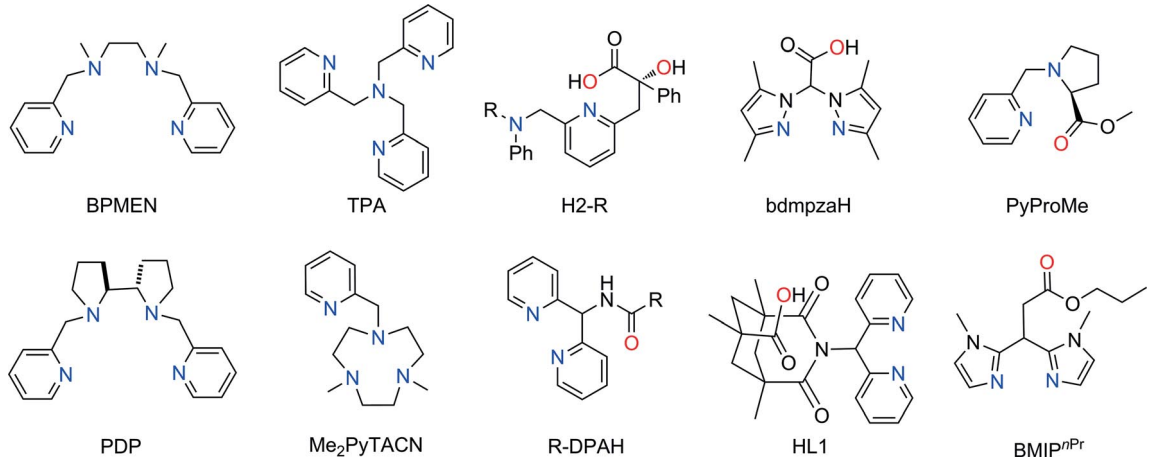


Figure 1. Selected ligands used for non-heme iron biomimetics.[6]

$Fe_2L_2$ dimeric complexes from the reaction with ferrous precursors.[21,30,31] The mono-ligand ferric complex $[Fe(bdmpza)Cl_3]$-$[NEt_4]$ has, to our knowledge never been applied as oxidation catalyst (Figure 1).[21] Furthermore, the R-DPAH ligand family developed by Que and co-workers and the polydentate pyridyl ligand from Bauer et al. resulted in bis-ligand complexes (Figure 1).[24,32]

By mimicking the active site of these iron enzymes more strictly, our group aims to develop new catalysts that allow further insights to be gained regarding the reactivity and the mechanism of operation of facial triad enzymes. To this end, we have previously reported the development of the tripodal 3,3-bis(alkylimidazol-2-yl)propionate (BAIP) N,N,O-ligand $BMIP^{nPr}$ (Figure 1).[33–35] This ligand and the corresponding carboxylate (BMIP) mimic the facial triad with two imidazole rings and a coordinating ester or carboxylate group, accurately modeling the two histidine and the aspartate or glutamate amino acids present in the enzymes.

To date, the use of these ligands mainly resulted in the formation of $[FeL_2]^{0/2+}$ complexes in which all six coordination sites around iron are occupied, similar to those reported by Burzlaff and Que. The neutral carboxylate complex $[Fe(BMIP)_2]$ displays no catalytic activity, whereas the cationic ester complex $[Fe(BMIP^{nPr})_2]^{2+}$ catalyzes the *cis*-dihydroxylation and epoxidation of olefins.[34,35] The latter is most probably facilitated by rearrangement and/or partial dissociation of the ligands in solution to create vacant sites on iron for catalysis to take place.

One way to overcome the formation of coordinatively saturated, homoleptic N,N,O-complexes is the addition of co-ligands. Making use of catechol co-ligands has previously allowed us to build structural and functional models for enzymes that are active in catechol cleavage.[36,37] In another attempt to overcome the formation of $FeL_2$ type complexes, a range of more bulky ligands was designed. This included variations in the ester moiety (*n*-propyl and *tert*-butyl), in the nitrogen substitution in the imidazole rings (methyl and ethyl), and in the substitution of the imidazole ring (imidazole, benzimidazole, and isopropyl-substituted imidazole).[33,35] However, none of these variations prevented the formation of $ML_2$ type complexes with both iron and copper.

In this work we present the new, slightly more bulky, methyl-substituted, benzimidazole ligands $BMB^{Me}IP^{nPr}$ and $BMB^{Me}IP$ (Figure 2). The additional methyl-substituents occupy a significant amount of space in the coordination environment because of the rigid benzimidazole scaffold. The use of these new ligands provides access to iron complexes comprising a single rigid tripodal N,N,O-ligand and readily available coordination sites, thereby leading to a closer mimic of the 2-His-1-carboxylate facial triad found in non-heme iron enzymes. The new complexes show catalytic turnover in the epoxidation of olefins with a slightly higher activity towards electron-rich substrates compared with electron-poor substrates.

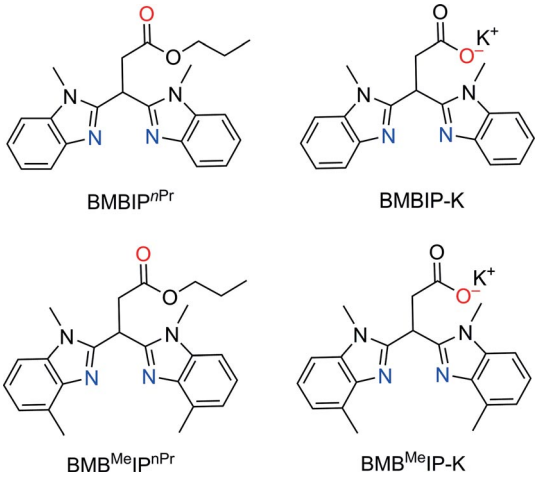


Figure 2. Overview of the ligands used in this study (from left to right): propyl 3,3-bis(1-methylbenzimidazol-2-yl)propionate ($BMBIP^{nPr}$), and potassium 3,3-bis(1-methylbenzimidazol-2-yl)propionate (BMBIP-K), and new ligands propyl 3,3-bis(1,5-dimethylbenzimidazol-2-yl)propionate ($BMB^{Me}IP^{nPr}$), and potassium 3,3-bis(1,5-dimethylbenzimidazol-2-yl)propionate ($BMB^{Me}IP$-K).

## Results and Discussion

### Design of a Bulky N,N,O-Ligand

From the X-ray crystal structure of $[Fe(BMBIP^{nPr})_2](OTf)_2$ it was observed that the benzimidazole rings of the two ligands approach each other quite closely.[35] Using this structure as the starting point, it seemed that additional methyl-substituents at the 5-position of both benzimidazoles would cause significant steric hindrance and could hamper the coordination of two N,N,O-ligands to a single metal center. At the same time, the relatively small methyl-substituents would leave enough space around the metal to keep it accessible for substrates and reactants for catalysis to take place. To test this, DFT calculations were carried out to explore whether the addition of methyl substituents would indeed prevent the formation of bis-ligand complexes.[38] The hypothetical equilibrium between an iron complex with two coordinated N,N,O-ligands and three non-coordinating water molecules and an iron complex with one tridentate ligand and three coordinated water molecules and one non-coordinating ligand was calculated (Scheme 1). From these calculations it was found that for the original benzimidazole ligand $BMBIP^{nPr}$ the equilibrium lies on the left side (the bis-ligand complex), similar to the structurally characterized complex with *cis*-positioned ligands.[35] The addition of methyl substituents as in ligand $BMB^{Me}IP^{nPr}$ shifts the equilibrium to the right side, favoring the formation of a mono-ligand complex. There is a significant difference in reaction enthalpy of 16 kcal/mol between these two equilibria. Based on these DFT calculations it was expected that the methyl-substituted ligand $BMB^{Me}IP^{nPr}$ would tend to form mono-ligand complexes, unlike $BMBIP^{nPr}$.

### Ligand Synthesis

The methyl-substituted ligand $BMB^{Me}IP^{nPr}$ was synthesized in three steps from the known phenylene diamine compound **5**. In total the ligand synthesis involved 6 steps as depicted in Scheme 2, this was performed on a multigram scale with an overall yield of 19%. The synthesis of **5** is based on several

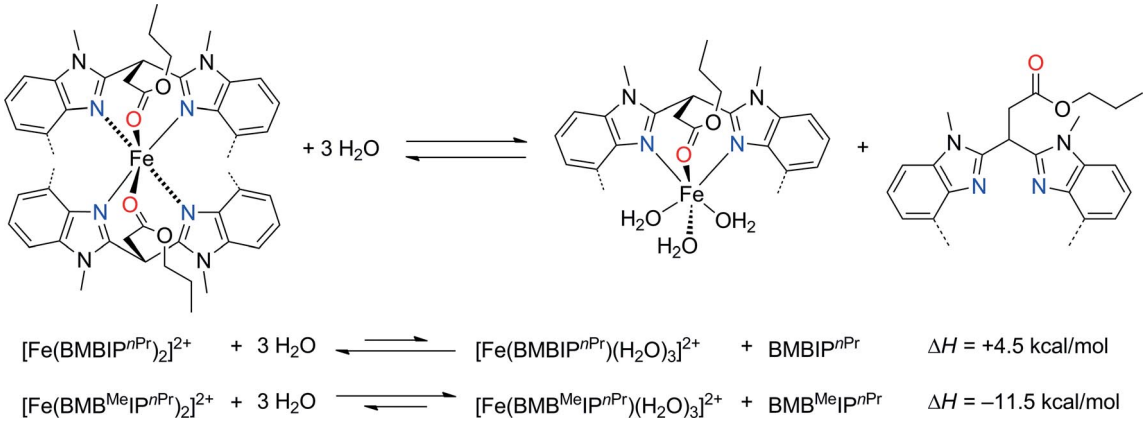


Scheme 1. The equilibria between bis- and mono-ligand iron complexes with $BMBIP^{nPr}$ ligands studied by DFT calculations. Functional: (U)BP86, basis set: 6-31* for C, H, N, and O and LANL2DZ for Fe. The dotted lines indicate a hydrogen or methyl substituent.

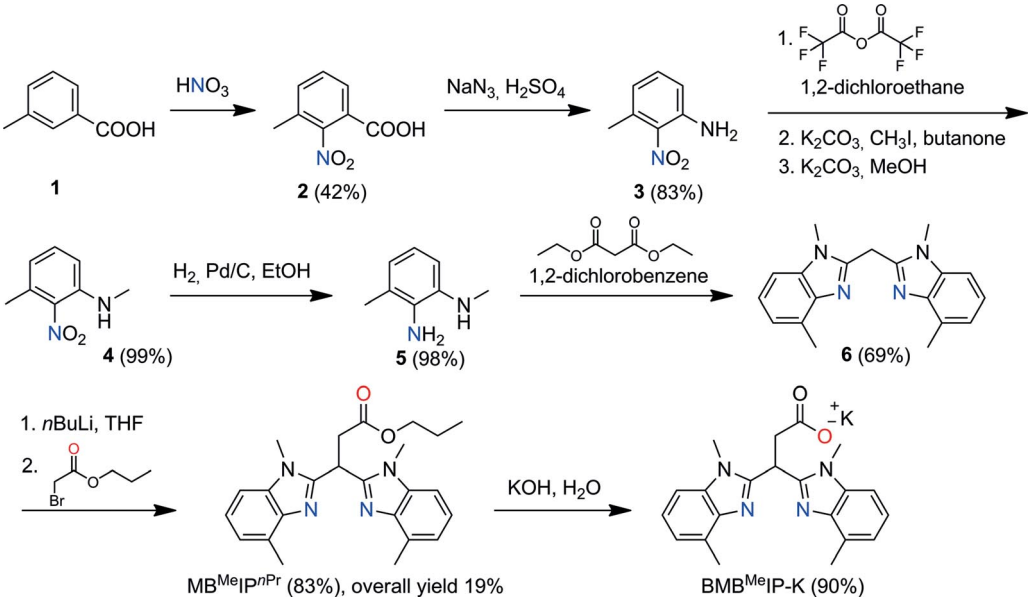


Scheme 2. Synthesis route towards $BMB^{Me}IP^{nPr}$ and $BMB^{Me}IP$-K.

reported procedures. Nitration of *m*-toluic acid (**1**) yielded **2** in 42 %,[39] followed by a Curtius rearrangement in which the carboxylic acid is converted into a primary amine group, giving **3** in 83 % yield.[40] The primary amine was then converted into a secondary amine in a methylation reaction to give **4**,[41] followed by hydrogenation of the nitro group to form **5** (both steps are quantitative). Benzimidazole ring closure with diethylmalonate gave bis(benzimidazolyl)methane **6** in 68 % yield.[42] Finally, lithiation of the methylene position in **6**, followed by alkylation with *n*-propylbromoacetate, based on the method published by Bruijnincx,[33] gave ligand BMB$^{Me}$IP$^{nPr}$ in 83 %. Saponification of the latter with KOH gave BMB$^{Me}$IP as the potassium salt (BMB$^{Me}$IP-K) in 90 % yield.

### NMR Study on Coordination Behavior

NMR experiments using various relative amounts (0.5, 1, and 2 equiv.) of the ligands BMB$^{Me}$IP$^{nPr}$, BMB$^{Me}$IP-K, BMBIP$^{nPr}$, and BMBIP-K with respect to Fe(OTf)$_2$•2MeCN were performed in CD$_3$CN. The carboxylate ligands are, in general, only sparingly soluble in acetonitrile, but the mixtures became clear upon mixing the ligand with iron triflate in all reactions, except for the reaction in which two equivalents of BMB$^{Me}$IP-K were used, which remained a suspension that was filtered before measurements were performed. Both $^1$H and $^{19}$F NMR spectra were recorded for all mixtures (see the Supporting Information).

In the case of the neutral ester ligands BMB$^{Me}$IP$^{nPr}$ and BMBIP$^{nPr}$, equilibrium mixtures containing two major species formed in CD$_3$CN solution. For BMB$^{Me}$IP$^{nPr}$ a small amount of free ligand was observed in all mixtures, the amount of which increased slightly with higher ligand loadings, whereas no free ligand was observed for BMBIP$^{nPr}$. As an example, the $^1$H NMR spectra for the experiments with BMB$^{Me}$IP$^{nPr}$ are shown in Figure 3, in which the two major species have their most indicative signals between 20 and 30 ppm (assignment in Figure S3). One of the species displays eight signals, indicating that the symmetry of the ligand is conserved upon coordination, and is assigned to a mono-ligated complex with the indicative peak at $\delta$ = 26.5 ppm. The second species displays 14 signals, indicating a bis-ligated complex, recognized as the peaks at $\delta$ = 24.7 and 22.8 ppm. Consistent with this analysis, the relative amount of the mono-ligand species increased from 35 to 74 % up to 92 % when the amount of ligand was decreased from 2 to 1 and 0.5 equiv. ligand with respect to iron.[43] For the less bulky BMBIP$^{nPr}$ ligand, the two major species show 7 and 18 signals, which are again assigned to mono- and bis-ligand species, respectively (Figure S4, assignment in Figure S6). With this ligand, near quantitative formation (96 %) of the bis-ligand complex was observed when two equivalents of ligand were present, which is consistent with previous results.[35] In the presence of an excess of iron, equimolar amounts of the two complexes form, showing the preference for the bis-ligand complex for BMBIP$^{nPr}$. The series of $^{19}$F NMR spectra using both types of neutral ligands range from a very broad signal with a full width half maximum (fwhm) larger than 2000 Hz when iron triflate is in excess, to a somewhat sharper signal (fwhm around 500 Hz) when the ligand is in excess (Figures S2 and S5). The observation of a single signal indicates exchange on the NMR timescale, with the broadening being due to relatively slow exchange and/or to paramagnetic broadening.

From these experiments it is concluded that the BMBIP$^{nPr}$ ligand tends to form a bis-ligand species, whereas BMB$^{Me}$IP$^{nPr}$ tends to form a mono-ligand species. These bis- and mono-ligand species can be formed with a selectivity of >90 %, and it is difficult to force the equilibria to the side of the disfavored product. For the bis-ligand product derived from the bulky BMB$^{Me}$IP$^{nPr}$ ligand, the proposed molecular structure involves two BMBIP$^{nPr}$ ligands acting as bidentate N,N-ligands with the ester moiety not coordinated to iron as reported earlier for a bulky imidazole-based BAIP ligand.[24]

To gain further insight into the equilibrium in the mixture with equimolar amounts of BMB$^{Me}$IP$^{nPr}$ and Fe(OTf)$_2$•2MeCN, variable-temperature $^1$H NMR measurements were performed. The ligand and Fe(OTf)$_2$•2MeCN were mixed in equimolar amounts, and measurements were performed at temperatures varying between –45 and 80 °C (Figure 4, and Figures S13 and S14). The relative amount of the mono-ligand species with respect to the bis-ligand species increased with increasing temperature. At –45 °C, the relative amount of mono-ligand species was around 55 %, and this increased to 95 % at 80 °C.[44] This result confirms the existence of a coordination equilibrium in acetonitrile solution. Furthermore, the signals are more paramagnetically shifted at lower temperatures, ruling out spin-crossover phenomena. A plot of the chemical shift vs. 1/*T* for

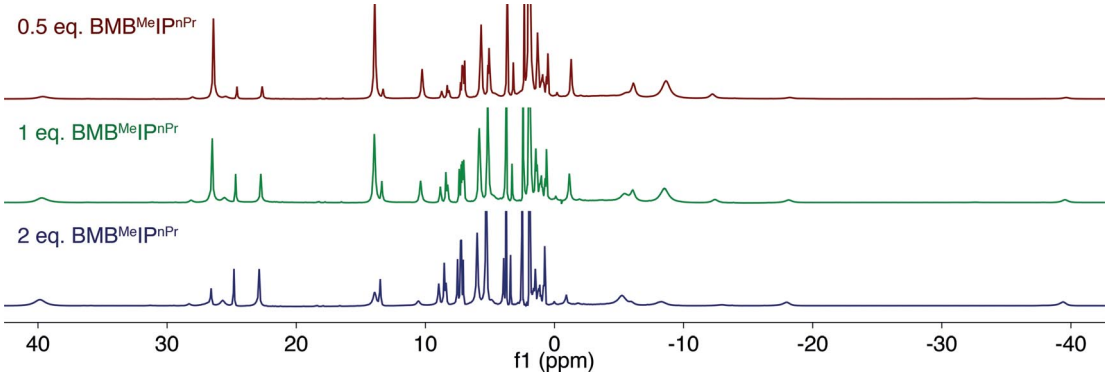


Figure 3. $^1$H NMR spectra of mixtures with various ratios of BMB$^{Me}$IP$^{nPr}$ and Fe(OTf)$_2$•2MeCN in CD$_3$CN. Top: 0.5 equiv.; middle: 1 equiv.; bottom: 2 equiv. of ligand with respect to iron.

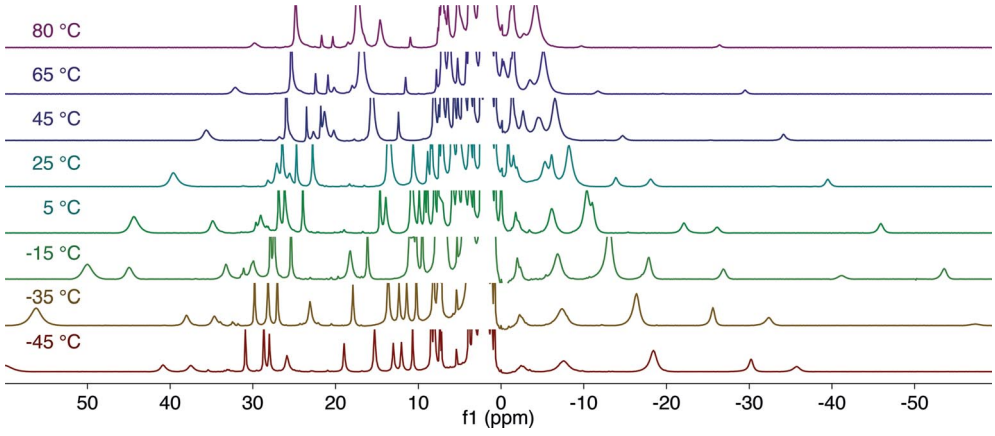


Figure 4. VT-$^1$H NMR experiment of a sample with equimolar amounts of $Fe(OTf)_2$•2MeCN and $BMB^{Me}IP^{nPr}$ with temperatures varying between –45 (bottom) and 80 °C (top) in $CD_3CN$.

the two characteristic signals for the bis-ligand complex (Figure S15) results in straight lines with intercepts of 4.8 and 6.3 ppm, which correspond to reasonable diamagnetic shifts, indicating normal Curie behavior. In contrast, for the mono-ligand complex, this plot deviates from linearity, suggesting that another chemical process [ligand exchange, reversible (de)coordination of the ester moiety] influences the temperature dependence of the chemical shift.

The set of NMR experiments with variable amounts of ligand was also carried out for the mono-anionic ligands $BMB^{Me}IP$-K and BMBIP-K. For $BMB^{Me}IP$-K, a small amount of free ligand was observed in all mixtures and this amount increased slightly with higher ligand loadings; for BMBIP-K, only a trace amount of ligand was observed. In the experiments with $BMB^{Me}IP$-K, the $^1$H NMR spectra of samples with 0.5 or 1 equiv. of ligand with respect to iron were very similar (Figure S7). Two species seem to be present, both giving 13 signals, with the major species, accounting for 85 %, assigned to a mono-ligand complex (assignment in Figure S9). The observation of 13 signals suggests that all 13 protons on the ligand are inequivalent except for the protons within the methyl groups. Furthermore it is expected that one or two acetonitrile molecules coordinate to the iron center to fill the coordination sphere, resulting in a complex with the overall formula $[Fe(BMB^{Me}IP)(OTf)(MeCN)_n]$ ($n$ = 1, 2, or 3). The minor species is proposed to result either from the formation of possible isomers or the formation of a dinuclear complex (see below). The addition of a second equivalent of ligand makes a substantial difference. As mentioned earlier, the NMR sample needed to be filtered before the measurement was performed. The resulting $^1$H NMR spectrum is completely different from the spectra of the mixtures with less ligand; weak paramagnetic peaks are present, which do not match with the species present in the other mixtures. A less well defined species seems to be formed in this reaction, possibly being a poorly soluble coordination oligo-/polymer, which has been observed before for similar ligands with zinc.[45]

For the smaller anionic ligand (BMBIP-K), the $^1$H NMR spectra with 0.5 and 1 equiv. ligand with respect to iron are again very similar, both showing around 50 weak paramagnetic signals, indicating a complex mixture of several compounds (Figure S10, assignment in S12). On the other hand, with two equivalents of this ligand, one major paramagnetic species with 12 signals is formed, indicating the formation of a well-defined complex.

The $^{19}$F NMR spectra show a similar trend for both types of anionic ligands: ranging from an extremely broad signal (fwhm = 3000 Hz) with an excess of iron triflate, to a sharp signal (fwhm = 6 Hz) with two equivalents of ligand (Figure S8 and S11). The sharp signal indicates that only non-coordinating triflate ions are present in the samples with two equivalents of an anionic ligand.

The measurements described above indicate that ligands $BMB^{Me}IP^{nPr}$ and $BMB^{Me}IP$ tend to form mono-ligand iron complexes of the type $[Fe(BMB^{Me}IP^{nPr})(OTf)_2]$ and $[Fe(BMB^{Me}IP)(OTf)(MeCN)_n]$ in contrast to $BMBIP^{nPr}$ and BMBIP, which tend to form the bis-ligand species $[Fe(BMBIP^{nPr})_2](OTf)_2$ and $[Fe(BMBIP)_2]$, respectively. The complexes bearing neutral ligands form equilibria in acetonitrile solution that shift upon changing the L/Fe ratio, whereas the complexes with anionic ligands form single, well-defined, complexes in solution.

## Isolation and Characterization of Iron(II) Complexes

The coordination properties of the new ligands $BMB^{Me}IP^{nPr}$ and $BMB^{Me}IP$ were further investigated by reactions with iron salts with strongly ($Cl^-$) and weakly coordinating ($OTf^-$) counterions, and isolation and further characterization of the obtained products. Furthermore, the products are compared to the products from the previously reported ligands $BMBIP^{nPr}$ and BMBIP.

## Coordination of Neutral $BMBIP^{nPr}$ and $BMB^{Me}IP^{nPr}$ Ligands

The neutral benzimidazole ligand $BMBIP^{nPr}$ is known to form the bis-ligand complex $[Fe(BMBIP^{nPr})_2](OTf)_2$ (**C**) when reacted with $Fe(OTf)_2$•2MeCN, as shown by Moelands.[35] However, upon mixing $FeCl_2$ with $BMBIP^{nPr}$ in methanol, the mono-ligand complex $[Fe(BMBIP^{nPr})Cl_2]$ (**A**) is formed. The pure product was obtained with a yield of 66 % by precipitation from the reaction mixture with diethyl ether (Scheme 3). The reaction of $FeCl_2$ with the more bulky, methyl-substituted benzimidazole ligand

($BMB^{Me}IP^{nPr}$) in methanol, resulted in the formation of a white precipitate; filtration provided [Fe($BMB^{Me}IP^{nPr}$)$Cl_2$] (**B**) in 41 % yield as a white powder (Scheme 3). Both chloride complexes were characterized by means of X-ray crystal structure determination, ESI-MS, IR, and $^1$H NMR spectroscopy.

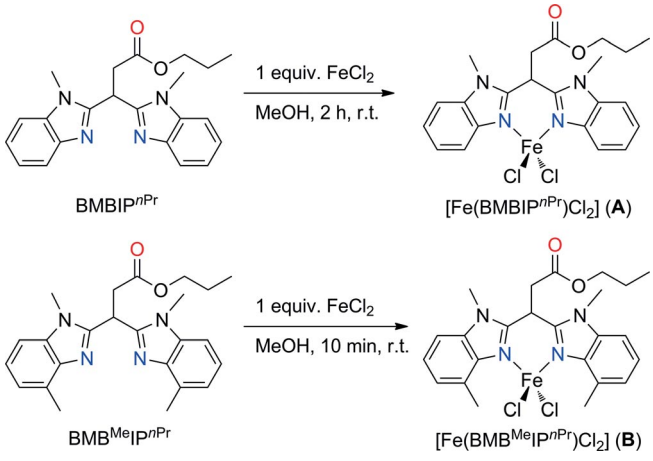


Scheme 3. Synthesis of [Fe($BMBIP^{nPr}$)$Cl_2$] (**A**) and [Fe($BMB^{Me}IP^{nPr}$)$Cl_2$] (**B**) from the coordination of $BMBIP^{nPr}$ and $BMB^{Me}IP^{nPr}$ to $FeCl_2$, respectively.

Complexes **A** and **B** are very similar to [Fe($BMIP^{nPr}$)$Cl_2$], which was obtained from the reaction of $FeCl_2$ with the parent methylimidazole-based ligand ($BMIP^{nPr}$).[46] Complex **B** crystallized with two independent molecules in the asymmetric unit. The molecular structures of **A** and one of the residues of **B** are shown in Figure 5 and selected bond lengths and angles of **A**, both residues of **B**, and [Fe($BMIP^{nPr}$)$Cl_2$] are given in Table S2. From the molecular structures it becomes clear that the carbonyl oxygen is not coordinated in these three complexes and that the ligands act as bidentate N,N-ligands instead of facial N,N,O-ligands. This is probably caused by electronic effects of the relatively strongly donating chloride ligands. All three structures have a distorted tetrahedral geometry with bite angles of 87.06(5), 92.00(6)/93.68(7), and 88.13(4)° for **A**, **B**, and [Fe($BMIP^{nPr}$)$Cl_2$], respectively. The slightly larger bite angles found in the two residues of **B** might be a consequence of steric interaction between the methyl substituents and the chloride ligands. The $C(H_3)$–Cl distances are found to be 3.630(3), 3.889(3), 3.675(3), and 3.879(3) Å, which are close to the sum of the van der Waals radius of Cl (1.75 Å)[47] and the radius of $CH_3$ (2.0 Å).[48] This might also cause the relatively large Cl1–Fe–Cl2 angles of 123.15(3) and 123.68(2)° in the two residues of this complex, compared with 115.770(18) and 117.743(15)° in the other two complexes. A spacefilling model plot is included in the Supporting Information (Figure S33). The Fe–N bond lengths range from 2.0703(12) to 2.1027(17) Å and are typical for high-spin iron(II) complexes. The longest bond lengths are found for the most bulky ligand. Furthermore, the Fe–Cl bond lengths within **B** differ significantly from each other by 0.0495(8) and 0.0408(8) Å, which makes this complex the least symmetrical.

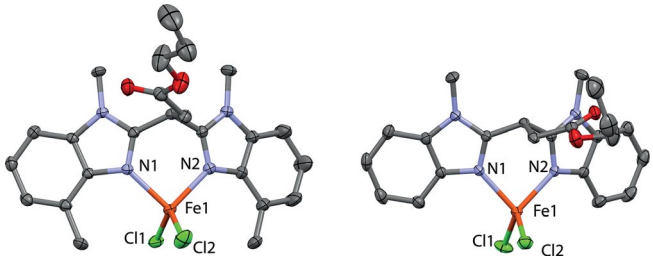


Figure 5. Molecular structures of [Fe($BMB^{Me}IP^{nPr}$)$Cl_2$] (**B**) Res1 (left) and [Fe($BMBIP^{nPr}$)$Cl_2$] (**A**) (right). Hydrogen atoms and non-coordinating solvent molecules are omitted for clarity. Displacement ellipsoids are drawn at the 50 % probability level.

The three chloride complexes were furthermore characterized by ESI-MS from acetonitrile solutions and all show the [M–Cl]$^+$ signal {*m/z* [Fe($BMB^{Me}IP^{nPr}$)Cl]: 495.1411 (calcd. 495.1251); [Fe($BMBIP^{nPr}$)Cl]: 467.0957 (calcd. 467.0938); [Fe($BMIP^{nPr}$)Cl]: 367.055 (calcd. 367.063)}. For **A**, an intense signal corresponding to [Fe($BMBIP^{nPr}$)$_2$Cl]$^+$ was also observed [*m/z* 843.2897 (calcd. 843.2838)]; whereas the corresponding ion was absent for **B**, although a small signal for the dimeric cation [$Fe_2$($BMB^{Me}IP^{nPr}$)$_2$-$Cl_3$]$^+$ was found [*m/z* 1027.2545 (calcd. 1027.2175)]. The NMR spectra of **A** and **B** in $CD_3CN$ both show a number of relatively sharp paramagnetically shifted peaks. Overall the spectra are similar to each other, with a sharp signal below 0 ppm and two intense signals between 20 and 30 ppm, the remaining signals are mainly found between 0 and 10 ppm (Figures S16 and S17). Both NMR spectra show fewer than the 10 signals that would be expected based on the number of protons present in the structures, indicating that some signals are either overlapping or too broad to observe. Only in the spectrum of **B** is a small amount of free ligand observed. Solid-state IR bands corresponding to C=O stretching vibrations found for the two chloride complexes match with non-coordinated carbonyl functionalities because they deviate from the corresponding free ligands by at most 22 cm$^{-1}$ (Table S1).

The ligand $BMBIP^{nPr}$ is known to form bis-ligand complex [Fe($BMBIP^{nPr}$)$_2$](OTf)$_2$ (**C**) (Scheme 4) from reaction with Fe(OTf)$_2$•2MeCN as reported before.[33] However, if the bulky methyl-substituted benzimidazole ligand ($BMB^{Me}IP^{nPr}$) is reacted with Fe(OTf)$_2$•2MeCN in methanol, the mono-ligand complex [Fe($BMB^{Me}IP^{nPr}$)(OTf)$_2$] (**D**) can be isolated (Scheme 4). A

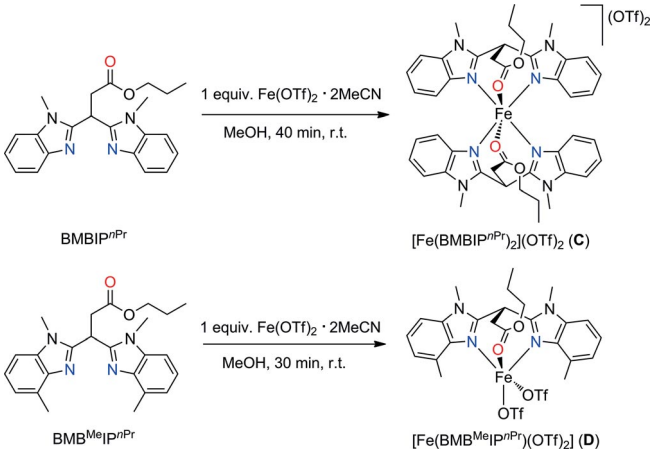


Scheme 4. Synthesis of [Fe($BMBIP^{nPr}$)$_2$](OTf)$_2$ (**C**) and [Fe($BMB^{Me}IP^{nPr}$)(OTf)$_2$] (**D**) from the coordination of $BMBIP^{nPr}$ and $BMB^{Me}IP^{nPr}$ to Fe(OTf)$_2$•2MeCN, respectively.

colorless $Fe(OTf)_2$ solution was added to a pale-brown solution containing an equimolar amount of the ligand and stirred for 30 min, after which the solvent was removed in vacuo and the off-white product was dissolved in an acetonitrile/diethyl ether mixture to precipitate the product as a dark-brown oil at –30 °C. Within weeks at –30 °C, light-brown crystals suitable for X-ray diffraction grew from this dark oil. The molecular structure of **D** shows a unique five-coordinate iron complex comprising one facial coordinating N,N,O-ligand and two coordinating triflate anions (Figure 6). Selected bond lengths and angles of **D** are given in Table 1.

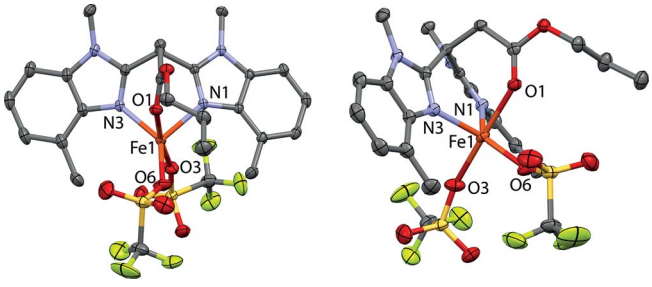


Figure 6. Two views of the molecular structure of $[Fe(BMB^{Me}IP^{nPr})(OTf)_2]$ (**D**). Hydrogen atoms and non-coordinating solvent molecules are omitted for clarity. Displacement ellipsoids are drawn at the 50 % probability level.

Table 1. Selected bond lengths and angles found for $[Fe(BMB^{Me}IP^{nPr})(OTf)_2]$ (**D**), BphC (1EIL.pdb), and DAOCS (1RXF.pdb).

| | **D** Bond length [Å] | BphC[50] Bond length [Å] | DAOCS[51] Bond length [Å] |
|---|---|---|---|
| Fe1–N1 | 2.0868(15) | 2.24 (His 145) | 2.19 (His 183) |
| Fe1–N3 | 2.0743(15) | 2.30 (His 209) | 2.15 (His 243) |
| Fe1–O1 | 2.1979(14) | 2.09 (Glu 260) | 2.15 (Asp 185) |
| Fe1–O3 | 2.1083(15) | 2.00 ($H_2O$ 743) | 2.11 ($H_2O$ 628) |
| Fe1–O6 | 1.9792(15) | 2.41 ($H_2O$ 622) | 2.23 ($H_2O$ 629) |
| Fe–O | | | 2.09 ($H_2O$ 630) |
| O1–C21 | 1.218(2) | 1.25 (Glu 260) | 1.26 (Asp 185) |
| | Angle [°] | Angle [°] | Angle [°] |
| N1–Fe1–N3 | 95.78(6) | 106.7 | 86.3 |
| O1–Fe1–N1 | 83.89(6) | 103.9 | 99.4 |
| O1–Fe1–N3 | 84.79(6) | 87.0 | 89.3 |
| O1–Fe1–O3 | 173.96(6) | 86.6 | 167.4 |
| N3–Fe1–O6 | 134.95(7) | 160.5 | 93.9 |
| O6–Fe1–N1 | 127.02(7) | 90.4 | 170.5 |
| O1–Fe1–O6 | 86.44(6) | 79.6 | 90.2 |

The geometry of **D** is best described as a distorted trigonal bipyramid ($\tau$ = 0.65)[49] with the coordinating ester group and one of the triflate ligands occupying the axial positions [O1–Fe–O3: 173.96(6)°]. The $BMB^{Me}IP^{nPr}$ ligand facially coordinates to the iron center as a tridentate N,N,O-ligand, the angles between the different arms of the ligand are found to be O1–Fe1–N3: 84.79(6)° and O1–Fe1–N1: 83.89(6)° and are quite close to 90°, as expected for a facial ligand. The N1–Fe–N3 bite angle of 95.78(6)° is indicative of the distorted trigonal bipyrimidal structure and is quite close to the bite angle of 92.00(7)° found in **B** with the same ligand. The Fe–N1/N3 bond lengths [2.0868(15)/2.0743(15) Å] are again typical for high-spin iron(II) complexes. Besides the N,N,O-ligand, two other coordination sites are occupied by weakly coordinating triflate ions. There is quite a large difference in the two Fe–OTf bond lengths, which are found to be 2.1083(15) and 1.9792(15) Å [Δ 0.129(2) Å]. The elongated Fe–O(3)Tf bond is found in the axial position *trans* to the coordinating ester moiety. The structure clearly shows that the two methyl substituents point away from the N,N,O-ligand scaffold towards the other half of the coordination sphere around iron, thereby blocking the coordination of a second ligand.

To provide a comparison between the five-coordinate structure of **D** and a typical 2-His-1-carboxylate facial triad in a mononuclear iron enzyme, its geometry around iron is compared to the active sites of two typical facial triad enzymes (Table 1, Figure 7). The first, 2,3-dihydroxybiphenyl dioxygenase (BphC), is an extradiol-type ring-cleavage dioxygenase and has a five-coordinate, square-pyramidal iron center.[50] The second, deacetoxycephalosporin C synthase (DAOCS), is active in the ring expansion of the thiazolidine ring of penicillin N and has a six-coordinate octahedral geometry.[51] The geometries of complex **D** and BphC are compared in the quaternion fit in Figure 7 (right). The iron centers in both enzymes only bear water molecules as ligands besides the facial N,N,O-coordination of the amino acids. An octahedral geometry around iron is often observed in enzymes; however, a five-coordinate TBP geometry is not uncommon for non-heme iron enzymes.[53] Furthermore, it is known that many enzymes become five-coordinate at the stage of catalysis, whereas they are six-coordinate in their resting state (which is not reactive towards dioxygen).[54]

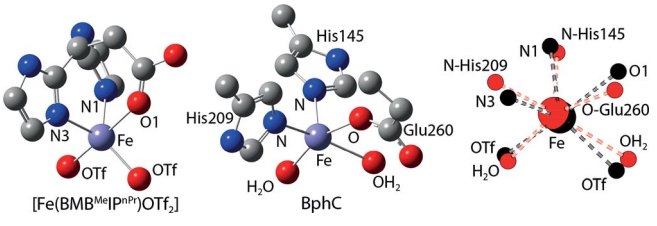


Figure 7. First coordination sphere of the iron center of **D** (left) and BphC (1EIL.pdb[50]) (middle). Quaternion fit[52] (right) of the iron and the donor atoms in the enzyme BphC (red) and complex **D** (black).

The average Fe–N bond lengths in **D** (ca. 2.08 Å) are found to be significantly shorter than the average in both enzymes (ca. 2.2 Å), whereas the Fe–O bond length is similar to that in DAOCS. The Fe–OTf bonds [Fe1–O3: 2.1083(15) and Fe1–O6: 1.9792(15) Å] are both found in the same range as the Fe–$OH_2$ bonds (2.00–2.41 Å).[50] The N1–Fe1–N3 bite angle is significantly larger in **D** [95.78(6)°] compared with that in DAOCS (86.3°); however, an even larger angle is found for BphC (106.7°) showing that this can also vary between enzymes. Besides this, the geometry of the N,N,O-coordination of the ligand comes very close to the N,N,O-motif in the enzymes.

Complex **D** is the first example of a ligand from the BAIP ligand family that does not form a bis-ligand iron complex from reaction with $Fe(OTf)_2$. In addition, it is the closest structural mimic to date of a typical five-coordinate 2-His-1-carboxylate facial triad active site, comprising a facial N,N,O-ligation of iron

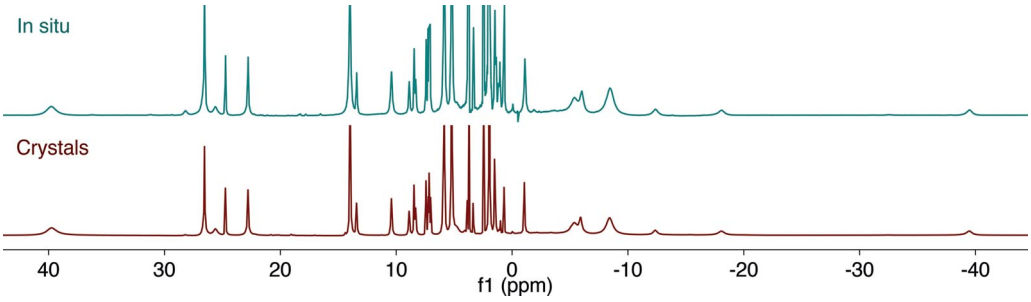


Figure 8. $^1$H NMR spectra in $CD_3CN$ from: Top: in situ mixing of $Fe(OTf)_2$•2MeCN and $BMB^{Me}IP^{nPr}$; Bottom: isolated crystals of **D**.

and easily exchangeable ligands that complete the coordination sphere around iron.

The structure and composition of **D** was further confirmed by ESI-MS, IR, and $^1$H and $^{19}$F NMR spectroscopy. The ESI-MS spectrum shows a $[Fe(BMB^{Me}IP^{nPr})(OTf)]^+$ ($[M–OTf]^+$) peak at *m/z* 609.1220 (calcd. 609.1082) and a signal for $[Fe(BMB^{Me}IP^{nPr})(OTf) + MeCN + H_2O]^+$ at *m/z* 668.1608 (calcd. 668.1453). These confirm the formation of a mono-ligand complex, and point to the lability of the triflate ligands and at the ability of the FeL unit to accommodate a total of three additional monodentate ligands. The $^1$H NMR spectrum of a $CD_3CN$ solution of isolated crystals is the same as the spectrum obtained from mixing equimolar amounts of $Fe(OTf)_2$•2MeCN with $BMB^{Me}IP^{nPr}$ (Figure 8). According to the number of peaks, there are two major and one minor paramagnetic species present as well as some free ligand. This suggests that the formation of different species in acetonitrile is an equilibrium process and involves the formation of small amounts of a bis-ligand complex as observed in the NMR studies (see above). Furthermore, the equilibrium might include coordination and dissociation of the triflate counterions and the coordinating carbonyl group. Finally, the $^{19}$F NMR spectrum shows a broad (fwhm = 1581 Hz) signal at –66 ppm typical for a coordinating or exchanging triflate ion.

The carbonyl absorption of **D** at 1699 cm$^{-1}$ is close to those of the other iron complexes in which the ester moiety coordinates to the iron center (Table S1). The lower Lewis acidic character of complex **D** compared with the cationic $[Fe(BAIP^R)_2]^{2+}$ complexes can explain the relatively small shift from the free ligand.

To conclude, three new iron complexes with neutral N,N,O-ligands have been synthesized: $[Fe(BMBIP^{nPr})Cl_2]$ (**A**), $[Fe(BMB^{Me}IP^{nPr})Cl_2]$ (**B**), and $[Fe(BMB^{Me}IP^{nPr})(OTf)_2]$ (**D**). All complexes bear only a single organic ligand. In the case of the chloride complexes, the stoichiometry is governed by the strongly coordinating character of the chloride anion that enforces a pseudotetrahedral 1:1 coordination for all ligands, notwithstanding the bulk of the ligand. In contrast, for triflate complexes, the specific design of the bulky ligand disfavors the formation of a bis-ligand complex similar to $[Fe(BMBIP^{nPr})_2](OTf)_2$ (**C**) and allows for the isolation of the mono-ligand complex $[Fe(BMB^{Me}IP^{nPr})(OTf)_2]$ (**D**). This is consistent with predictions from DFT calculations (see above), which pointed out a strong influence of the additional methyl groups in $BMB^{Me}IP^{nPr}$ on coordination equilibria.

## Coordination of the Anionic $BMB^{Me}IP$ Ligand

Even though the ester ligand $BMB^{Me}IP^{nPr}$ described above acts as a facial tridentate N,N,O-ligand, being a close mimic of the 2-His-1-carboxylate facial triad, it does not mimic the negatively charged carboxylate group from a coordinating aspartate or glutamate that is commonly present in the 2-His-1-carboxylate facial triad. In that sense, the mono-anionic ligand $BMB^{Me}IP$ can result in even better enzyme mimics. Furthermore, $BMB^{Me}IP$ binds more strongly to the iron center, preventing the establishment of coordination equilibria.

The related mono anionic ligands BMIP and BMBIP are known to form neutral, bis-ligand complexes with copper(II) ions, as was published by Bruijnincx et al.[33] Furthermore, studies on the coordination of the mono-anionic parent ligand BMIP to iron have also been reported.[34,55] The reaction of BMIP with $Fe(OTf)_2$•2MeCN results in the formation of $[Fe(BMIP)_2]$, which is isostructural to $[Cu(BMBIP)_2]$.[33]

Upon addition of $BMB^{Me}IP$-K to a solution of $Fe(OTf)_2$•2MeCN in acetonitrile, the ligand, which itself is insoluble in acetonitrile, gradually dissolved within a few minutes, indicating the formation of a metal complex (Scheme 5). After a few hours, a fine white precipitate formed, which was removed by filtration. Drying of the filtrate gave an off-white powder in quantitative yield. The product was analyzed by ESI-MS, IR, $^1$H and $^{19}$F NMR spectroscopy.

ESI-MS analysis of the product showed three major signals at *m/z* 417.0994 (calcd. 417.1008), 437.6157 (calcd. 437.6141), and 983.1545 (calcd. 983.1550) corresponding to $[Fe_2(BMB^{Me}IP)_2]^{2+}$, $[Fe_2(BMB^{Me}IP)_2 + MeCN]^{2+}$, and $[Fe_2(BMB^{Me}IP)_2 + OTf]^+$, all being a dimer of the target compound. Additionally, a minor peak was observed at *m/z* 605.0251 (calcd. 605.0172) corresponding to the target compound $[Fe(BMB^{Me}IP)(OTf) + K]^+$ and no peaks in the spectrum could be assigned to a mononuclear bis-ligand complex. The formation of dimers might take place during the measurement or they might be easier to observe because the target compound is neutral. Based on this, it is not possible to establish whether a mono- or dinuclear complex is formed. A dimeric complex similar to $[Fe(bdtbpza)Cl]_2$, in which carboxylate groups coordinate in a $\kappa^1\mu$-fashion, bridging between two iron centers, is unlikely due to geometric constrains.[20,21] Another possibility is the formation of a dinuclear complex in which the nitrogen atoms of one ligand coordinate to a different iron center than the oxygen in which both the mono- and bidentate coordination modes of the carboxylate groups are

 

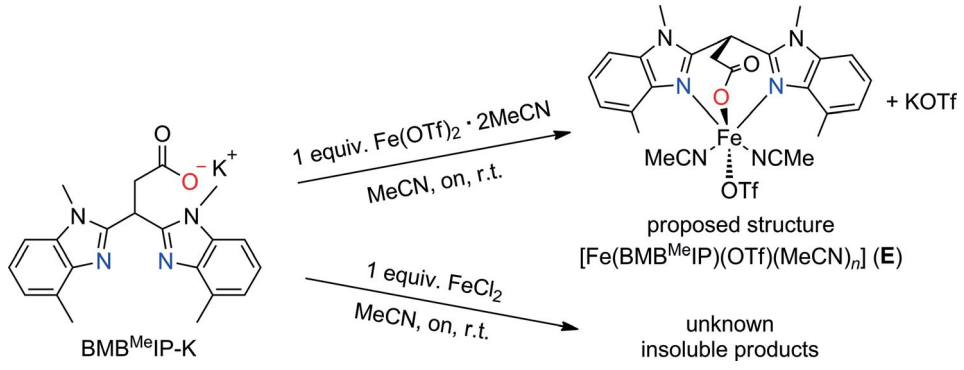


Scheme 5. Reaction scheme for the coordination of BMB$^{Me}$IP to $FeCl_2$ and $Fe(OTf)_2$·2MeCN and the proposed structure of the obtained product [Fe(BMB$^{Me}$IP)(OTf)(MeCN)$_n$] (**E**).

possible. In the IR spectrum, the asymmetric stretching vibration of the carboxylate group is found at 1582 cm$^{-1}$, which is very close in energy to that of BMB$^{Me}$IP-K (1581 cm$^{-1}$) and of the bis-ligand iron and copper complexes [Fe(BMIP)$_2$] and [Cu(BMBIP)$_2$] (1580 cm$^{-1}$). The difference between the asymmetric and symmetric vibrations is indicative of the coordination mode of the carboxylate group. If the difference [$\Delta(\nu_{as} - \nu_s)$] decreases compared with the free carboxylate ligand, the coordination approaches $C_{2v}$ symmetry; if it increases, this in indicative of a monodentate coordination mode of the carboxylate.[56,57] The symmetric stretching vibration of the carboxylate group is tentatively assigned to the signal at 1393 cm$^{-1}$ (BMB$^{Me}$IP-K: 1384 cm$^{-1}$), which results in a $\Delta(\nu_{as} - \nu_s)$ of 190 cm$^{-1}$. This difference is smaller than 198 cm$^{-1}$ found for BMB$^{Me}$IP-K, but in the range found for a free carboxylic acid.[58] These IR data are not conclusive for the coordination (mode) of the carboxylate group. Attempts to optimize the geometry of a mononuclear complex with a chelating carboxylate group by DFT all failed. The expected ring strain for a chelating carboxylate means that a monodentate coordination mode of the carboxylate is proposed for a mononuclear complex. However, in a dinuclear or oligomeric structure chelation could still be possible. From the shouldered vibrations found for the triflate ions (1279/1253, 1225, 1175/1160, 1031, and 637/631 cm$^{-1}$), it is clear that a mixture of coordinating and non-coordinating triflate ions is present, suggesting that attempts to completely remove the KOTf side product failed thus far. $^1$H NMR spectroscopy shows 13 major peaks and another set of 13 minor peaks, similar to the spectrum discussed before (see above) (Figure S20). The major complex is assigned to the mono-ligand complex with one coordinating triflate ion and presumably two coordinating acetonitrile molecules (**E**). The minor complex is proposed to be either an isomer or a dinuclear complex. The $^{19}$F NMR spectrum shows a somewhat broadened peak (fwhm = 73 Hz) for the triflate anion, indicating that it is at least partially coordinating to an iron center. In the case of $FeL_2$ type complexes with non-coordinating triflate counterions, a sharp fluorine signal typical for free triflate ions is observed.[34] This supports the notion that a mono-ligand complex is also obtained in case of the carboxylate ligand; however, the (simultaneous) formation of dinuclear species with an overall 1:1 ligand to iron ratio cannot be ruled out. The proposed structure of the mononuclear complex is that of a mono-ligand, mono-triflate, bis-acetonitrile adduct with the overall formula [Fe(BMB$^{Me}$IP)(OTf)(MeCN)$_n$] (**E**), which is present in two geometric isomers.

From the reaction of BMB$^{Me}$IP-K and $FeCl_2$ in acetonitrile, an off-white precipitate with a very low solubility was obtained (Scheme 5). Despite the low solubility, ESI-MS analysis showed a predominant signal at *m/z* 491.0275 (calcd. 491.0340) corresponding to [Fe(BMB$^{Me}$IP)Cl + K]$^+$. A dilute $^1$H NMR spectrum, measured from the crude reaction mixture in $CD_3CN$, indicated the presence of one major paramagnetic species. The IR spectrum showed the $\nu CO_s$ and $\nu CO_{as}$ vibrations at 1599 and 1372 cm$^{-1}$, respectively, resulting in a $\Delta(\nu_{as} - \nu_s)$ of 227 cm$^{-1}$, which is significantly larger than 198 cm$^{-1}$ found for BMB$^{Me}$IP-K and is indicative of a monodentate coordination mode of the carboxylate group. The low solubility of the product hampered further analysis.

Based on the data obtained on reactions of BMB$^{Me}$IP-K with iron salts, it is proposed that also with this anionic carboxylate ligand, a well-defined mono-ligand iron complex is obtained from its reaction with $Fe(OTf)_2$·2MeCN with the overall formulation [Fe(BMB$^{Me}$IP)(OTf)(MeCN)$_n$] (**E**). It is less clear which product is formed from the reaction of this ligand with $FeCl_2$. Unfortunately all attempts to obtain high-quality crystals from either of the complexes with the mono-anionic carboxylate (BMB$^{Me}$IP) ligand yielded either dendritic crystals or noncrystalline material.

## Epoxidation Catalysis

The new BMB$^{Me}$IP ligands, unlike the BMBIP ligands, tend to form mono-ligand iron complexes ([Fe(BMB$^{Me}$IP$^{nPr}$)(OTf)$_2$] (**D**) and [Fe(BMB$^{Me}$IP)(OTf)(MeCN)$_n$] (**E**)) with three readily available coordination sites on iron. This makes the resulting iron complexes good structural models of the 2-His-1-carboxylate facials triad. To investigate whether these complexes are also functional models, the iron complexes bearing BMB$^{Me}$IP ligands were studied as catalysts for the oxidation of olefins. To date, there is no example of an iron complex bearing a single mono-anionic facial N,N,O-ligand showing catalytic activity in the oxidation of olefins (see the Introduction).

Initial testing of **D** and **E** [in situ mixing of ligand and $Fe(OTf)_2$·2MeCN; Supporting Information: Catalysis Data, Opti-

mization of Catalytic Conditions] in the oxidation of benchmark substrates *cis*-cyclooctene and styrene with $H_2O_2$ showed that mainly the epoxide products are obtained (Tables 2 and 3). With *cis*-cyclooctene, trace amounts of *cis*-1,2-cyclooctanediol are formed. No formation of 1-phenyl-1,2-ethanediol is observed in the oxidation of styrene; instead a significant amount of benzaldehyde is formed. Initial testing of the chloride complexes did not result in catalytic turnover numbers, therefore their activity was not investigated further.

Table 2. Oxidation of *cis*-cyclooctene by iron complexes bearing N,N,O-ligands with $H_2O_2$.[a]

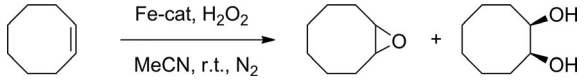


| Entry | Ligand (equiv.) | TON epoxide 1 h | TON epoxide 21 h | TON diol 21 h | $H_2O_2$ conv. [%] 21 h[b] |
|---|---|---|---|---|---|
| 1[c] | BMB$^{Me}$IP-K (1) | 1.1 | 2.8 | 0.1 | 2.9 |
| 2 | BMB$^{Me}$IP-K (2) | 0.5 | 1.3 | 0.1 | 1.4 |
| 3[c,d] | BMB$^{Me}$IP$^{nPr}$ (1) | 2.2 | 5.8 | 0.2 | 6.0 |
| 4 | BMB$^{Me}$IP$^{nPr}$ (2) | 1.2 | 2.6 | 0.1 | 2.7 |
| 5[e] | BMBIP-K (1) | 1.9 | 3.6 | 0.2 | 3.8 |
| 6 | BMBIP-K (2) | 0.7 | 1.8 | 0.2 | 2.0 |
| 7[d] | BMBIP$^{nPr}$ (1) | 2.9 | 6.1 | 0.3 | 6.4 |
| 8[f] | BMBIP$^{nPr}$ (2) | 3.1 | 4.6 | 1.5 | 6.1 |

[a] Reaction conditions: ligand (3 μmol), iron triflate (3 μmol), *cis*-cyclooctene (3 mmol), MeCN (5 mL), r.t., $H_2O_2$ (0.6 M, 0.5 mL added over 20 min by using a syringe pump), $N_2$ atmosphere. Catalyst/substrate/oxidant ratio, 1:1000:100. The products were analyzed by GC and the amounts were calculated by using 1,2-dibromobenzene as the internal standard. TON in mol product/mol catalyst. [b] Productive $H_2O_2$ conversion is based on the conversion of $H_2O_2$ into epoxides and *cis*-1,2-cyclooctanediol. [c] Averaged over four runs. [d] Some background activity of free $Fe(OTf)_2$ is expected and can account for 25–30 % of the observed catalytic activity; a more detailed discussion and control experiments are included in the Supporting Information. [e] Averaged over two runs. [f] These numbers are slightly different from previously published results.[34] This can be explained by the difference between using an isolated catalyst or an in situ generated catalyst.

Under optimized conditions (Tables S3 and S4), complex **E** shows catalytic activity in the epoxidation of both *cis*-cyclooctene and styrene, reaching over 1 TON within 1 h (Table 2 and Table 3, entry 1). The reactions continued overnight, resulting in TONs up to 4.6 after 21 h. With **D**, TONs of 2.2 and 0.8 were obtained in 1 h for *cis*-cyclooctene and styrene, respectively, and these increased to 5.8 and 3.6 in 21 h (entry 3 in Table 2 and Table 3). The TONs towards the epoxide products are of the same order of magnitude for both substrates. However, for styrene, benzaldehyde is formed as the main product in significantly higher amounts than the epoxide, resulting in higher productive consumption of $H_2O_2$. Quite surprisingly, the reactions continued for more than a week, and iodometric titrations of the reaction mixtures after several days show that $H_2O_2$ is still present, showing that disproportionation of $H_2O_2$ is not significant.

To investigate the effect of a second ligand on the catalytic activity, reactions were also performed with two equivalents of ligand relative to iron triflate and using all four benzimidazole ligands (Figure 2). For *cis*-cyclooctene, it was found that the reactivity halves with two equivalents of BMB$^{Me}$IP-K, BMB$^{Me}$IP$^{nPr}$, and BMBIP-K (Table 2, entries 2, 4, and 6), whereas with two

Table 3. Oxidation of styrene by iron complexes bearing N,N,O-ligands with $H_2O_2$.[a]

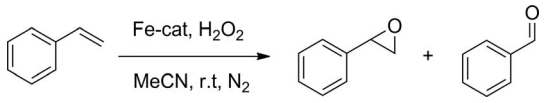


| Entry | Ligand (equiv.) | TON epoxide 1 h | TON epoxide 21 h | TON aldehyde 21 h | $H_2O_2$ conv. [%] 21 h[b] |
|---|---|---|---|---|---|
| 1[c] | BMB$^{Me}$IP-K (1) | 1.4 | 4.6 | 8.2 | 12.8 |
| 2 | BMB$^{Me}$IP-K (2) | 1.1 | 4.8 | 7.6 | 12.4 |
| 3[d,e] | BMB$^{Me}$IP$^{nPr}$ (1) | 0.8 | 3.6 | 10.2 | 13.9 |
| 4 | BMB$^{Me}$IP$^{nPr}$ (2) | 1.5 | 4.6 | 10.0 | 14.6 |
| 5[d] | BMBIP-K (1) | 3.0 | 6.9 | 8.7 | 15.6 |
| 6 | BMBIP-K (2) | 1.0 | 5.1 | 8.5 | 13.6 |
| 7[e] | BMBIP$^{nPr}$ (1) | 4.2 | 8.0 | 10.6 | 18.6 |
| 8 | BMBIP$^{nPr}$ (2) | 6.1 | 8.7 | 11.4 | 20.2 |

[a] Reaction conditions: ligand (3 μmol), iron triflate (3 μmol), styrene (3 mmol), MeCN (5 mL), r.t., $H_2O_2$ (0.6 M , 0.5 mL, added over 20 min by using a syringe pump), $N_2$ atmosphere. Catalyst/substrate/oxidant ratio, 1:1000:100. The products were analyzed by GC and the amounts were calculated by using 1,2-dibromobenzene as the internal standard. TON in mol product/mol catalyst. [b] Productive $H_2O_2$ conversion is based on the conversion of $H_2O_2$ into epoxides and benzaldehyde. [c] Averaged over three runs. [d] Averaged over two runs. [e] Some background activity of free $Fe(OTf)_2$ is expected and can account for 25–30 % of the observed catalytic activity; a more detailed discussion and control experiments are included in the Supporting Information.

equivalents of non-bulky ester ligand BMBIP$^{nPr}$ a slight increase of the initial reactivity is observed together with a significant increase in diol formation (entry 8). When styrene was used as the substrate, different trends were found. In this case, the addition of a second equivalent of the bulky carboxylate ligand BMB$^{Me}$IP-K influences the reactivity of the catalyst very little (Table 3, entry 2). In contrast, using two equivalents of non-bulky carboxylate BMBIP-K results in a three times lower activity compared with the use of one equivalent of ligand (entry 6). For both ester ligands, the TONs for styrene increase with a factor of 1.5 when a second equivalent of the ligand is present (entries 4 and 8).

General observations in these series of catalytic experiments are that the overall activity decreases with a second equivalent of ligand (exceptions are the use of ester ligands in reactions with styrene; see below), that carboxylate ligands tend to result in species with lower activity, and that the increased bulk of the new methyl-substituted ligands results in a decrease in overall activity. The first trend is likely a consequence of the formation of coordinatively saturated complexes without available sites on the iron center. For example, for isolated $[Fe(BMIP)_2](OTf)_2$ it is known that it shows no activity at all.[34] The formation of an $FeL_2$ type saturated complex is unfavorable for the more bulky ligand BMB$^{Me}$IP and, as expected, the decrease in catalytic activity upon the addition of a second equivalent of BMB$^{Me}$IP is less pronounced. However, the proposed formation of coordination oligomers in these cloudy catalytic mixtures can also block a part of the coordination sites or precipitate iron compounds out of solution, resulting in reduced catalytic activity. Next to iron speciation, steric and electronic ligand effects may also affect substrate approach and the inherent reactivity of active

species involved in catalysis and may therefore contribute to the general reactivity trends.

The increased diol formation observed in the oxidation reaction of *cis*-cyclooctene with two equivalents of BMBIP$^{nPr}$ type ligands (Table 2, entry 8) can be explained by the possible dissociation of the weakly coordinating ester moieties from an $FeL_2$ type complex. This creates vacant sites on the iron center and results in an $N_4$-coordination sphere around iron, similar to other homogeneous non-heme iron catalysts active in the epoxidation and *cis*-dihydroxylation of olefins.[14,59,60] We have earlier proposed similar active species for iron-based olefin oxidation catalysts bearing two neutral N,N,O-ligands from the BAIP ligand family, for example [Fe(BMIP$^{nPr}$)$_2$](OTf)$_2$.[34,35] The increase in the amount of diol products upon the addition of a second equivalent of ligand is not observed for mixtures containing the bulky ester ligand BMB$^{Me}$IP$^{nPr}$ (entry 4), suggesting the formation of a different active species. Similar considerations on the coordination of two ester ligands can explain the increase in styrene conversion when two equivalents of ligand are applied.

Finally, the substrate scope was extended and four additional substrates were tested: *p*-OMe and *p*-Cl styrene, *trans*-chalcone, and 1-octene (Table S5). When comparing the three styrene substrates, it is found that both [Fe(BMB$^{Me}$IP)(OTf)(MeCN)$_n$] (**E**) and [Fe(BMB$^{Me}$IP$^{nPr}$)(OTf)$_2$] (**D**) show the highest reactivity with electron-rich substrates (*p*-OMe styrene). The reactivity towards the more electron-poor substrates *p*-Cl styrene and chalcone is relatively low. Hardly any conversion of the terminal alkene 1-octene is obtained. The preference for an electron-rich substrate indicates an electrophilic nature of the metal-based oxidant that is generated in these reactions.

The catalytic activity of complexes **D** and **E** supports the idea that a mononuclear iron complex with a single facial N,N,O-ligand is active in the oxidation of olefins. Que et al. have reported the mono-ligand complex [Fe(**L1**)X] (X = Cl or OTf) (Figure 1), which showed only stoichiometric reactivity of the iron complex in the epoxidation and *cis*-dihydroxylation of alkenes.[19] Que et al. furthermore published the catalytic activity of a series of complexes of the [Fe(R-DPAH)$_2$]$^{2+}$ family (Figure 1), which have a strong selectivity towards the formation of diols with TONs up to 9.4 for styrene.[22,24] For these complexes, the active species is proposed to have a 1:1 iron/ligand ratio; however, no hard evidence for this is provided. Our group previously reported the activity of [Fe(PyProMe)Cl$_2$] in the epoxidation of olefins with TONs up to 50, but the flexible structure of this ligand allows isomerization to meridional coordination, which makes the structure of the active species uncertain.

## Conclusions

We have developed BMB$^{Me}$IP and BMB$^{Me}$IP$^{nPr}$ as new ligands in the BAIP series, which are slightly more bulky than previously published ligands and enabled us to obtain mono-ligand iron complexes. Three new iron complexes with neutral N,N,O-ligands are synthesized: [Fe(BMBIP$^{nPr}$)Cl$_2$] (**A**), [Fe(BMB$^{Me}$IP$^{nPr}$)Cl$_2$] (**B**), [Fe(BMB$^{Me}$IP$^{nPr}$)(OTf)$_2$] (**D**) as well as [Fe(BMB$^{Me}$IP)(OTf)(MeCN)$_n$] (**E**) with an anionic ligand. All complexes bear only a single ligand per iron, and no $FeL_2$ type complexes are formed.

The new [Fe(BMB$^{Me}$IP$^{nPr}$)(OTf)$_2$] complex, with a biologically relevant tridentate facial N,N,O-ligand and easily exchangeable monodentate co-ligands, represents to our knowledge the closest structural mimic to date of the 2-His-1-carboxylate facial triad. Additionally, it is the first example of a ligand from the BAIP ligand family that tends to form a mono- instead of bis-ligand iron complex from reactions with Fe(OTf)$_2$, leaving three coordination sites readily available for reactions to take place. For [Fe(BMB$^{Me}$IP)(OTf)(MeCN)$_n$], a very similar structure is proposed but exact structural comparison was not possible because of the lack of a crystal structure. We have shown that these model complexes are catalytically active (TON > 1) in the epoxidation of olefins. This shows that an iron center supported by a single facial N,N,O-ligand, mimicking the active site of non-heme iron enzymes, is active in the epoxidation of olefins. General trends in these catalytic epoxidations show the enhanced reactivity of mono-ligand iron complexes and point out that ligand bulk (BMB$^{Me}$IP vs. BMBIP) and electronics (ester vs. carboxylate) influences the overall reactivity.

The coordination chemistry of the bulky N,N,O-ligands reported here and related ones, as well as the activity of the new complexes in other reactions performed by enzymes with the 2-His-1-carboxylate facial triad is under investigation.

## Experimental Section

**General:** The synthesis of iron-containing compounds and other air- and moisture-sensitive reactions were performed under an oxygen-free nitrogen atmosphere using standard Schlenk or glovebox techniques. Air-sensitive materials and samples were weighed in an MBraun labmaster dp glovebox workstation. For all air- and moisture-sensitive reactions, dried and degassed solvents were used. The solvents diethyl ether, tetrahydrofuran, acetonitrile, and hexane were dried with an MBraun MB SPS-800 solvent purification system. Methanol and dichloromethane were dried with magnesium turnings and $CaH_2$, respectively, and distilled under nitrogen prior to use. Ligands BMBIP$^{nPr}$ and BMBIP-K were prepared on a multigram scale according to the previously published procedures starting from the commercially available 1-methylbenzimidazole.[33,35] The metal precursor iron triflate was synthesized according to a reported procedure.[61] All other reagents and solvents were obtained commercially and used without further purification. Column chromatography was performed using silica gel (60–200 μm). $^1$H, $^{19}$F, and $^{13}$C NMR spectra were recorded with a 400 MHz Varian spectrometer at 25 °C (unless stated differently). Chemical shifts are reported in ppm with respect to tetramethylsilane (TMS) based on the position of residual solvent peaks as reported by Fulmer et al.[62] IR spectra were recorded with a Perkin–Elmer Spectrum One FTIR spectrometer and ESI-MS measurements were performed with a Waters LCT Premier XE KE317. GC analysis was performed with a Perkin–Elmer Clarus 500 Gas Chromatograph equipped with an Agilent HP-5 column (30 m × 0.32 mm × 0.25 μm) and a flame-ionization detector. Experimental details on the ligand synthesis are included in the Supporting Information.

CCDC 1422425 (for [Fe(BMB$^{Me}$IP$^{nPr}$)Cl$_2$]), 1422426 (for [Fe(BMBIP$^{nPr}$)Cl$_2$]), 1422427 (for [Fe(BMIP$^{nPr}$)Cl$_2$]), 1422428 (for [Fe(BMB$^{Me}$IP$^{nPr}$)(OTf)$_2$]), and 1422429 (for [H$_2$BMB$^{Me}$IP$^{nPr}$][OTf]$_2$ + [HBMB$^{Me}$IP$^{nPr}$][OTf]) contain the supplementary crystallographic data for this paper. These data can be obtained free of charge from The Cambridge Crystallographic Data Centre.

**NMR Studies:** The ligand ($BMB^{Me}IP^{nPr}$, $BMB^{Me}IP$-K, $BMBIP^{nPr}$, and BMBIP-K) and $Fe(OTf)_2$•2MeCN were mixed in the required stoichiometry (L/Fe; 1:2, 1:1, and 2:1) in $CD_3CN$. In the case of the neutral ligands, the ligand as well as $Fe(OTf)_2$•2MeCN dissolve easily in $CD_3CN$ upon which they react. The anionic ligands are insoluble but upon reaction with $Fe(OTf)_2$•2MeCN, the mixtures become clear. The only exception is the reaction of two equivalents of $BMB^{Me}IP$-K with $Fe(OTf)_2$•2MeCN, which resulted in a suspension that was filtered before measurements were made. Both $^1H$ and $^{19}F$ NMR spectra were recorded for all mixtures. In all spectra from the mixtures with $BMB^{Me}IP^{nPr}$ and $BMB^{Me}IP$ a small amount of free ligand was observed, with the amount of free ligand increasing only slightly with higher L/Fe ratios. In the case of $BMBIP^{nPr}$, no free ligand was observed. Trace amounts of BMBIP were observed in the corresponding experiments.

**[$Fe(BMIP^{nPr})Cl_2$]:** $FeCl_2$ (131 mg, 1.03 mmol) in methanol (7 mL) was added to a stirring solution of $BMIP^{nPr}$ (288 mg, 1.04 mmol) in methanol (7 mL) and the reaction mixture was stirred for 1 h at room temperature. The solvent was evaporated in vacuo and the remaining yellow solid was recrystallized from an acetonitrile/diethyl ether mixture at –30 °C. The product was obtained as a slightly yellowish crystalline solid (354 mg, 85 %). Crystals suitable for X-ray diffraction were obtained by slow vapor-diffusion of diethyl ether into an acetonitrile solution. ESI-MS (acetonitrile): *m/z* 367.055 {[M – Cl]$^+$, calcd. 367.063}. IR (solid): $\tilde{\nu}$ = 3121.8, 2964.6, 1727.2, 1628.1, 1547.8, 1503.3, 1467.5, 1396.9, 1364.1, 1279.0, 1196.3, 1180.4, 1159.5, 1140.3, 982.9, 969.4, 765.7, 741.0 cm$^{-1}$. Solution magnetic moment (Evans' method): $\mu_{eff}$ = 5.2 $\mu_B$. X-ray crystal structure determination: $C_{14}H_{20}Cl_2FeN_4O_2$; Fw = 403.09; pale-yellow plate; 0.36 × 0.36 × 0.15 mm$^3$; monoclinic; $P2_1/c$ (no. 14); $a$ = 10.05732(12), $b$ = 15.8041(3), $c$ = 14.8005(3) Å, $\beta$ = 129.172(2)°; $V$ = 1823.77(7) Å$^3$; $Z$ = 4; $D_x$ = 1.468 g/cm$^3$; $\mu$ = 1.13 mm$^{-1}$. 34899 Reflections were measured on a Nonius Kappa CCD diffractometer with rotating anode and graphite monochromator ($\lambda$ = 0.71073 Å) at a temperature of 150(2) K up to a resolution of (sin $\theta/\lambda)_{max}$ = 0.65 Å$^{-1}$. The intensities were integrated with the Eval14 software.[63] A numerical absorption correction and scaling was performed with SADABS[64] (correction range 0.63–0.85). 4182 Reflections were unique ($R_{int}$ = 0.016), of which 3841 were observed [$I > 2\sigma(I)$]. The structure was solved with Direct Methods using SHELXS-97.[65] Least-squares refinement was performed with SHELXL-2014[66] against $F^2$ of all reflections. Non-hydrogen atoms were refined freely with anisotropic displacement parameters. All hydrogen atoms were located in difference Fourier maps and refined with a riding model. 212 Parameters were refined with no restraints. $R_1/wR_2$ [$I > 2\sigma(I)$]: 0.0225/0.0574. $R_1/wR_2$ [all refl.]: 0.0259/0.0594, $S$ = 1.029. Residual electron density between –0.24 and 0.37 e/Å$^3$. Geometry calculations and checking for higher symmetry was performed with the PLATON program.[67]

**[$Fe(BMBIP^{nPr})Cl_2$] (A):** A colorless solution of $FeCl_2$ (22 mg, 0.17 mmol) in methanol (3 mL) was added to a yellow solution of $BMBIP^{nPr}$ (65 mg, 0.17 mmol) in methanol (3 mL). Resulting in a slightly darker, yellowish brown solution. The reaction mixture was stirred for 2 h, after which part of the solvent was evaporated and diethyl ether (5 mL) was added to precipitate the product as an off-white powder. The solution was removed with a cannula filter and the precipitate was washed with diethyl ether (3 × 2 mL) to yield an off-white product (58 mg, 66 %). Vapor diffusion of diethyl ether into an acetonitrile solution of the product resulted in crystals suitable for X-ray crystallography. $^1H$ NMR (400 MHz, $CD_3CN$, 25 °C): $\delta$ = –35.90, –5.56, –0.08, 0.97, 3.79, 10.57, 20.49, 23.41, 29.82 ppm. ESI-MS (acetonitrile): *m/z* = 467.0957 {[M–Cl]$^+$, calcd. 467.0938}, 843.2897 {[$Fe(BMBIP^{nPr})_2$ + Cl]$^+$, calcd. 843.2838}. IR (KBr): $\tilde{\nu}$ = 2965.0 (w), 2359.6 (m), 1732.0 (s), 1494.4 (s), 1458.3 (s), 1265.4 (m), 1188.7 (m), 748.5 (m) cm$^{-1}$. X-ray crystal structure determination: $C_{22}H_{24}Cl_2FeN_4O_2$ + disordered solvent; Fw = 503.20;[68] yellow needle; 0.48 × 0.06 × 0.06 mm$^3$; monoclinic; $P2_1/c$ (no. 14); $a$ = 9.7644(4), $b$ = 16.2321(13), $c$ = 16.8394(6) Å, $\beta$ = 106.516(2)°; $V$ = 2558.9(2) Å$^3$; $Z$ = 4; $D_x$ = 1.306 g/cm$^3$;[68] $\mu$ = 0.82 mm$^{-1}$.[68] 39413 Reflections were measured on a Bruker Kappa ApexII diffractometer with sealed tube and Triumph monochromator ($\lambda$ = 0.71073 Å) at a temperature of 150(2) K up to a resolution of (sin $\theta/\lambda)_{max}$ = 0.65 Å$^{-1}$. The intensities were integrated with the Eval15 software.[69] Multiscan absorption correction and scaling was performed with SADABS[64] (correction range 0.66–0.75). 5875 Reflections were unique ($R_{int}$ = 0.031), of which 4849 were observed [$I > 2\sigma(I)$]. The structure was solved with Direct Methods using SHELXS-97.[65] Least-squares refinement was performed with SHELXL-2013[66] against $F^2$ of all reflections. The crystal structure contains large solvent accessible voids (310 Å$^3$/unit cell) filled with severely disordered solvent molecules. Their contribution to the structure factors was taken into account with the Squeeze algorithm[70] resulting in 89 electrons/unit cell. Non-hydrogen atoms were refined freely with anisotropic displacement parameters. Hydrogen atoms were introduced in calculated positions and refined with a riding model. The *n*-propyl group was refined with a disorder model. 292 Parameters were refined with two restraints (distances in the disordered group). $R_1/wR_2$ [$I > 2\sigma(I)$]: 0.0287/0.0687. $R_1/wR_2$ [all refl.]: 0.0394/0.0727, $S$ = 1.018. Residual electron density between –0.30 and 0.34 e/Å$^3$. Geometry calculations and checking for higher symmetry was performed with the PLATON program.[67]

**[$Fe(BMB^{Me}IP^{nPr})Cl_2$] (B):** A colorless solution of $FeCl_2$ (22 mg, 0.17 mmol) in methanol (3 mL) was added to a light-brown solution of $BMB^{Me}IP^{nPr}$ (70 mg, 0.17 mmol) in methanol (5 mL). A white precipitate formed and the brown supernatant was removed by cannula filtration. The precipitate was washed with methanol (3 × 2 mL) to give a white solid (37 mg, 41 %). Vapor diffusion of diethyl ether into a THF solution resulted in crystals suitable for X-ray diffraction. $^1H$ NMR (400 MHz, $CD_3CN$, 25 °C): $\delta$ = –1.50, 0.50, 1.23, 3.37, 4.40, 6.89, 22.78, 26.10 ppm. ESI-MS (THF): *m/z* = 495.1411 {[M–Cl]$^+$, calcd. 495.1251}, 1027.2545 {[2Fe + $2BMB^{Me}IP^{nPr}$ + 3Cl]$^+$, calcd. 1027.2175}. IR (KBr): $\tilde{\nu}$ = 2971.4 (m), 2359.9 (w), 1746.4 (s), 1601.7 (m), 1494.6 (s), 1458.2 (m), 1412.7 (m), 1262.9 (m), 1236.0 (m), 1196.0 (s), 1074.2 (m), 1062.0 (m), 972.18 (w), 760.4 (m) cm$^{-1}$. Solution magnetic moment (Evans' method): $\mu_{eff}$ = 4.9 $\mu_B$. X-ray crystal structure determination: $C_{24}H_{28}Cl_2FeN_4O_2$ + disordered solvent; Fw = 531.25;[68] colorless needle; 0.59 × 0.16 × 0.06 mm$^3$; triclinic; $P\bar{1}$ (no. 2); $a$ = 12.6110(4), $b$ = 15.0668(6), $c$ = 16.7815(6) Å, $\alpha$ = 70.088(2), $\beta$ = 80.401(2); $\gamma$ = 77.759(2)°; $V$ = 2914.27(19) Å$^3$; $Z$ = 4; $D_x$ = 1.211 g/cm$^3$;[68] $\mu$ = 0.73 mm$^{-1}$.[68] 48699 Reflections were measured on a Bruker Kappa ApexII diffractometer with sealed tube and Triumph monochromator ($\lambda$ = 0.71073 Å) at a temperature of 150(2) K up to a resolution of (sin $\theta/\lambda)_{max}$ = 0.65 Å$^{-1}$. The intensities were integrated with the Eval15 software[69] using a model for large anisotropic mosaicity about *hkl* = (1,0,0). Multiscan absorption correction and scaling was performed with SADABS[64] (correction range 0.63–0.75). 13383 Reflections were unique ($R_{int}$ = 0.035), of which 10059 were observed [$I > 2\sigma(I)$]. The structure was solved with Direct Methods using SHELXS-97.[65] Least-squares refinement was performed with SHELXL-2013[66] against $F^2$ of all reflections. The crystal structure contains large solvent accessible voids (597 Å$^3$/unit cell) filled with severely disordered THF and diethyl ether molecules. Their contribution to the structure factors was taken into account with the Squeeze algorithm[70] resulting in 151 electrons/unit cell. Non-hydrogen atoms were refined freely with anisotropic displacement parameters. Hydrogen atoms were introduced in cal-

culated positions and refined with a riding model. 604 Parameters were refined with no restraints. $R_1/wR_2$ [$I > 2\sigma(I)$]: 0.0381/0.0953. $R_1/wR_2$ [all refl.]: 0.0575/0.1026, $S$ = 1.053. Residual electron density between –0.42 and 0.73 e/Å$^3$. Geometry calculations and checking for higher symmetry was performed with the PLATON program.[67]

**[Fe(BMB$^{Me}$IP$^{nPr}$)(OTf)$_2$] (D):** A colorless solution of Fe(OTf)$_2$•2MeCN (0.434 g, 0.997 mmol) in methanol (5 mL) was added to a pale-brown solution of BMB$^{Me}$IP$^{nPr}$ (0.403 g, 1.00 mmol) in methanol (15 mL). After 30 min of stirring, the solvent was removed in vacuo and the resulting off-white solid was dissolved in acetonitrile/diethyl ether for recrystallization at –30 °C. The product precipitated as dark-brown oil and the supernatant was removed. After weeks at –30 °C, clear crystals suitable for X-ray crystallography, formed from this brown oil. $^1$H NMR (400 MHz, CD$_3$CN, 25 °C): $\delta$ = –39.52, –18.07, –12.40, –8.45, –5.93, –5.35, –1.07, 1.5, 2.44, 3.70, 5.22, 5.84, 7.42, 8.32, 8.46, 8.88, 10.41, 13.41, 13.97, 22.78, 24.73, 25.57, 26.54, 39.77 ppm. ESI-MS (acetonitrile): $m/z$ = 405.2220 {[L + H]$^+$, calcd. 405.2291}, 609.1220 {[M–OTf]$^+$, calcd. 609.1082}, 668.1608 {[M–OTf + MeCN + H$_2$O]$^+$, calcd. 668.1453}, 809.4616 {[2L + H]$^+$, calcd. 809.4503}. IR (KBr): $\tilde{\nu}$ = 2969.4 (m), 2877.0 (w), 1732.2 (m), 1698.8 (m), 1604.0 (w), 1498.7 (m), 1460.7 (w), 1330.1 (m), 1308.4 (m), 1243.4 (s), 1211.8 (s), 1187.0 (m), 1176.9 (m), 1027.9 (s), 782.9 (m), 753.5 (m), 634.1 (s), 512.5 (m) cm$^{-1}$. X-ray crystal structure determination: C$_{26}$H$_{28}$F$_6$FeN$_4$O$_8$S$_2$•CH$_3$CN; Fw = 799.55; brown needle; 0.31 × 0.09 × 0.08 mm$^3$; triclinic; $P\bar{1}$ (no. 2); $a$ = 10.2193(9), $b$ = 11.2508(10), $c$ = 15.8601(15) Å, $\alpha$ = 93.244(3), $\beta$ = 92.104(3); $\gamma$ = 112.484(3)°; $V$ = 1678.8(3) Å$^3$; $Z$ = 2; $D_x$ = 1.582 g/cm$^3$; $\mu$ = 0.66 mm$^{-1}$. 28036 Reflections were measured on a Bruker Kappa ApexII diffractometer with sealed tube and Triumph monochromator ($\lambda$ = 0.71073 Å) at a temperature of 150(2) K up to a resolution of (sin $\theta/\lambda)_{max}$ = 0.65 Å$^{-1}$. The intensities were integrated with the Saint software.[71] Multiscan absorption correction and scaling was performed with SADABS[64] (correction range 0.71–0.75). 7716 Reflections were unique ($R_{int}$ = 0.027), of which 6154 were observed [$I > 2\sigma(I)$]. The structure was solved with Patterson superposition methods using SHELXT.[72] Least-squares refinement was performed with SHELXL-2012[66] against $F^2$ of all reflections. Non-hydrogen atoms were refined freely with anisotropic displacement parameters. All hydrogen atoms were located in difference Fourier maps and refined with a riding model. 457 Parameters were refined with no restraints. $R_1/wR_2$ [$I > 2\sigma(I)$]: 0.0352/0.0847. $R_1/wR_2$ [all refl.]: 0.0509/0.0918, $S$ = 1.021. Residual electron density between –0.45 and 0.48 e/Å$^3$. Geometry calculations and checking for higher symmetry was performed with the PLATON program.[67]

**[Fe(BMB$^{Me}$IP)(OTf)(MeCN)$_n$] (E):** BMB$^{Me}$IP-K (135 mg, 0.336 mmol) and Fe(OTf)$_2$•2MeCN (147 mg, 0.336 mmol) were mixed in acetonitrile (5 mL). Upon stirring, the solids quickly dissolved, resulting in a clear slightly brown solution. After stirring for 7 h at room temperature, a fine white precipitate formed which was removed by filtration. The filtrate was dried in vacuo, yielding the product as an off-white powder (266 mg, quant.). The product still contained some KOTf. $^1$H NMR (400 MHz, CD$_3$CN, 25 °C): $\delta$ = –32.85, –28.92, –18.47, –13.82, –8.19, –6.10, –2.01, 0.47, 1.26, 5.40, 6.61, 8.02, 9.45, 10.14, 17.79, 18.35, 20.44, 26.72, 27.92, 31.78, 35.51, 38.98, 45.64, 47.12, 105.44, 108.53 ppm. ESI-MS (acetonitrile): $m/z$ = 417.0994 {[2Fe + 2BMB$^{Me}$IP]$^{2+}$, calcd. 417.1008}, 437.6157 {[2Fe + 2BMB$^{Me}$IP + MeCN]$^{2+}$, calcd. 437.6141}, 605.0251 {[M + K]$^+$, calcd. 605.0172}, 983.1545 {[2Fe + 2BMB$^{Me}$IP + OTf]$^+$, calcd. 983.1550}. IR (KBr): $\tilde{\nu}$ = 3061.4 (w), 2972.2 (w), 1582.0 (m), 1501.3 (w), 1449.5 (w), 1422.0 (w), 1393.0 (w), 1252.5 (s), 1225.3 (s), 1175.3 (m), 1078.5 (w), 1030.6 (s), 779.2 (m), 746.82 (m), 637.1 (s), 631.6 (s), 575.4 (m), 516.5 (m) cm$^{-1}$.

**[Fe(BMB$^{Me}$IP)Cl]:** BMB$^{Me}$IP-K (54.3 mg, 0.136 mmol) and FeCl$_2$ (17.6 mg, 0.139 mmol) were mixed in acetonitrile (3 mL). Upon stirring, the solids partially dissolved and immediately a fine white precipitate formed. The precipitate is collected by filtration and the product was obtained as a barely soluble white powder (57.8 mg, 94 %). $^1$H NMR (400 MHz, CD$_3$CN, 25 °C): $\delta$ = –6.24, –4.24, –1.92, 3.53, 4.95, 7.41, 22.77, 23.18 ppm. ESI-MS (acetonitrile): $m/z$ = 491.0275 {[M – K]$^+$, calcd. 491.0340}. IR (KBr): $\tilde{\nu}$ = 3055.7 (w), 2952.5 (w), 2923.2 (w), 1599.1 (m), 1490.3 (s), 1455.0 (m), 1371.8 (m), 1233.2 (m), 1075.0 (w), 986.6 (w), 884.1 (w), 870.4 (w), 781.5 (m), 744.5 (s), 702.3 (w), 643.9 (w), 563.8 (w), 507.7 (w) cm$^{-1}$.

**Catalysis Protocol:** The ligand (3 µmol or 6 µmol) and iron Fe(OTf)$_2$•2MeCN (3 µmol) were reacted in acetonitrile (4.5 mL) at room temperature under N$_2$ atmosphere, resulting in a clear, slightly brown solution within a few minutes. The substrate (typically 1000 equiv., 3 mmol) and 1,2-dibromobenzene (10 µL, 83 µmol, internal standard) were then added, followed by 0.5 mL H$_2$O$_2$ (typically: 100 equiv., 300 µmol, 0.6 M solution in acetonitrile diluted from 35 % aqueous H$_2$O$_2$) dropwise in 20 min by using a syringe pump. The reaction was stirred at room temperature and, after 30 min, the first sample (0.5 mL) was taken followed by samples after 1, 2, and 21 h. The samples were diluted with diethyl ether (1 mL) and analyzed by GC (HPLC in the case of chalcone). The products were identified and quantified by comparison to authentic compounds.

## Acknowledgments

The authors would like to thank the Dutch National Research School Combination-Catalysis Controlled by Chemical Design (NRSC – Catalysis) for their financial support. M.-E. M. acknowledges funding from the European Union Seventh Framework Programme (FP7/2007-2013) under grant agreement PIIF-GA-2012-327306 (IIF-Marie Curie grant) and Utrecht University (Tenure-track grant, Sectorplan Natuur- en Scheikunde). M. O. acknowledges a grant from Utrecht University within the sustainability theme. The DFT work was carried out on the Dutch national e-infrastructure with the support of the SURF Foundation. The X-ray diffractometer has been financed by the Netherlands Organization for Scientific Research (NWO).

**Keywords:** Enzyme models · Metalloenzymes · Iron · N,O ligands · Epoxidation · Non-heme iron

[1] M. Costas, M. P. Mehn, M. P. Jensen, L. Que Jr., *Chem. Rev.* **2004**, *104*, 939–986.
[2] L. Que Jr., *Nat. Struct. Biol.* **2000**, *7*, 182–184.
[3] E. L. Hegg, L. Que Jr., *Eur. J. Biochem.* **1997**, *250*, 625–629.
[4] K. D. Koehntop, J. P. Emerson, L. Que Jr., *J. Biol. Inorg. Chem.* **2005**, *10*, 87–93.
[5] P. C. A. Bruijnincx, G. van Koten, R. J. M. Klein Gebbink, *Chem. Soc. Rev.* **2008**, *37*, 2716–2744.
[6] BPMEN [*N,N'*-dimethyl-*N,N'*-bis(2-pyridylmethyl)-1,2-diaminomethane], PDP [*N,N'*-bis(2-pyridylmethyl)-2,2'-bipyrrolidine], TPA [tris(picolyl)-amine], Me$_2$PyTACN [1-(2'-pyridylmethyl)-4,7-dimethyl-1,4,7-triazacyclononane], H2-R ((*S*)-3-{6-[(alkyl-phenylamino)-methyl]pyridin-2-yl}-2-hydroxy-2-phenylpropionic acid), R-DPAH (*N*-acylated dipyridin-2-yl-methylamine), bdmpzaH [bis(3,5-dimethylpyrazol-1-yl)acetic acid], HL1 [3-(dipyridin-2-yl-methyl)-1,5,7-trimethyl-2,4-dioxo-3-azabicyclo[3.3.1]-nonane-7-carboxylic acid], PyProMe [(*S*)-methyl-1-(pyridin-2-yl-methyl)pyrrolidine-2-carboxylate], BMIP$^{nPr}$ [propyl 3,3-bis(1-methylimidazol-2-yl)propionate].

[7] E. P. Talsi, K. P. Bryliakov, *Coord. Chem. Rev.* **2012**, *256*, 1418–1434.
[8] K. P. Bryliakov, E. P. Talsi, *Coord. Chem. Rev.* **2014**, *276*, 73–96.
[9] M. Costas, K. Chen, L. Que Jr., *Coord. Chem. Rev.* **2000**, *200–202*, 517–544.
[10] A. Company, L. Gómez, X. Fontrodona, X. Ribas, M. Costas, *Chem. Eur. J.* **2008**, *14*, 5727–5731.
[11] I. Prat, A. Company, V. Postils, X. Ribas, L. Que Jr., J. M. Luis, M. Costas, *Chem. Eur. J.* **2013**, *19*, 6724–6738.
[12] I. Prat, A. Company, T. Corona, T. Parella, X. Ribas, M. Costas, *Inorg. Chem.* **2013**, *52*, 9229–9244.
[13] L. Gómez, M. Canta, D. Font, I. Prat, X. Ribas, M. Costas, *J. Org. Chem.* **2013**, *78*, 1421–1433.
[14] I. Prat, D. Font, A. Company, K. Junge, X. Ribas, M. Beller, M. Costas, *Adv. Synth. Catal.* **2013**, *355*, 947–956.
[15] M. S. Chen, M. C. White, *Science* **2007**, *318*, 783–787.
[16] M. S. Chen, M. C. White, *Science* **2010**, *327*, 566–572.
[17] P. J. Cappillino, J. R. Miecznikowski, L. A. Tyler, P. C. Tarves, J. S. McNally, W. Lo, B. S. T. Kasibhatla, M. D. Krzyaniak, J. McCracken, F. Wang, W. H. Armstrong, J. P. Caradonna, *Dalton Trans.* **2012**, *41*, 5662–6577.
[18] O. Cussó, X. Ribas, J. Lloret-Fillol, M. Costas, *Angew. Chem. Int. Ed.* **2015**, *54*, 2729–2733; *Angew. Chem.* **2015**, *127*, 2767.
[19] P. D. Oldenburg, C.-Y. Ke, A. A. Tipton, A. A. Shteinman, L. Que Jr., *Angew. Chem. Int. Ed.* **2006**, *45*, 7975–7978; *Angew. Chem.* **2006**, *118*, 8143.
[20] A. Beck, B. Weibert, N. Burzlaff, *Eur. J. Inorg. Chem.* **2001**, 521–527.
[21] A. Beck, A. Barth, E. Hübner, N. Burzlaff, *Inorg. Chem.* **2003**, *42*, 7182–7188.
[22] P. Oldenburg, A. A. Shteinman, L. Que Jr., *J. Am. Chem. Soc.* **2005**, *127*, 15672–15673.
[23] S. J. Friese, B. E. Kucera, L. Que Jr., W. B. Tolman, *Inorg. Chem.* **2006**, *45*, 8003–8005.
[24] P. D. Oldenburg, Y. Feng, I. Pryjomska-Ray, D. Ness, L. Que Jr., *J. Am. Chem. Soc.* **2010**, *132*, 17713–17723.
[25] A. Gonzalez-de-Castro, J. Xiao, *J. Am. Chem. Soc.* **2015**, *137*, 8206–8218.
[26] S. M. Barry, H. Mueller-Bunz, P. J. Rutledge, *Org. Biomol. Chem.* **2012**, *10*, 7372–7381.
[27] S. M. Barry, P. J. Rutledge, *Synlett* **2008**, 2172–2174.
[28] M. A. H. Moelands, D. J. Schamhart, E. Folkertsma, M. Lutz, A. L. Spek, R. J. M. Klein Gebbink, *Dalton Trans.* **2014**, *43*, 6769–6785.
[29] S. Gosiewska, J. J. L. M. Cornelissen, M. Lutz, A. L. Spek, G. van Koten, R. J. M. Klein Gebbink, *Inorg. Chem.* **2006**, *45*, 4214–4227.
[30] A. Otero, J. Fernández-Baeza, A. Lara-Sánchez, L. F. Sánchez-Barba, *Coord. Chem. Rev.* **2013**, *257*, 1806–1868.
[31] N. Burzlaff, *Adv. Inorg. Chem.* **2008**, *60*, 101–165.
[32] M. Lenze, S. L. Sedinkin, E. B. Bauer, *J. Mol. Catal. A* **2013**, *373*, 161–171.
[33] P. C. A. Bruijnincx, M. Lutz, A. L. Spek, E. E. van Faassen, B. M. Weckhuysen, G. van Koten, R. J. M. Klein Gebbink, *Eur. J. Inorg. Chem.* **2005**, 779–787.
[34] P. C. A. Bruijnincx, I. L. C. Buurmans, S. Gosiewska, M. A. H. Moelands, M. Lutz, A. L. Spek, G. van Koten, R. J. M. Klein Gebbink, *Chem. Eur. J.* **2008**, *14*, 1228–1237.
[35] M. A. H. Moelands, S. Nijsse, E. Folkertsma, B. de Bruin, M. Lutz, A. L. Spek, R. J. M. Klein Gebbink, *Inorg. Chem.* **2013**, *52*, 7394–7410.
[36] P. C. A. Bruijnincx, M. Lutz, A. L. Spek, W. R. Hagen, B. M. Weckhuysen, G. van Koten, R. J. M. Klein Gebbink, *J. Am. Chem. Soc.* **2007**, *129*, 2275–2286.
[37] P. C. A. Bruijnincx, M. Lutz, A. L. Spek, W. R. Hagen, G. van Koten, R. J. M. Klein Gebbink, *Inorg. Chem.* **2007**, *46*, 8391–8402.
[38] M. J. Frisch, G. W. Trucks, H. B. Schlegel, G. E. Scuseria, M. A. Robb, J. R. Cheeseman, G. Scalmani, V. Barone, B. Mennucci, G. A. Petersson, H. Nakatsuji, M. Caricato, X. Li, H. P. Hratchian, A. F. Izmaylov, J. Bloino, G. Zheng, J. L. Sonnenberg, M. Hada, M. Ehara, K. Toyota, R. Fukuda, J. Hasegawa, M. Ishida, T. Nakajima, Y. Honda, O. Kitao, H. Nakai, T. Vreven, J. A. Montgomery, Jr., J. E. Peralta, F. Ogliaro, M. Bearpark, J. J. Heyd, E. Brothers, K. N. Kudin, V. N. Staroverov, R. Kobayashi, J. Normand, K. Raghavachari, A. Rendell, J. C. Burant, S. S. Iyengar, J. Tomasi, M. Cossi, N. Rega, J. M. Millam, M. Klene, J. E. Knox, J. B. Cross, V. Bakken, C. Adamo, J. Jaramillo, R. Gomperts, R. E. Stratmann, O. Yazyev, A. J. Austin, R. Cammi, C. Pomelli, J. W. Ochterski, R. L. Martin, K. Morokuma, V. G. Zakrzewski, G. A. Voth, P. Salvador, J. J. Dannenberg, S. Dapprich, A. D. Daniels, Ö. Farkas, J. B. Foresman, J. V. Ortiz, J. Cioslowski, D. J. Fox, *Gaussian 09*, revision D.01, Gaussian, Inc., Wallingford, CT, USA, **2013**.
[39] S. Kanoh, H. Muramoto, N. Kobayashi, M. Motoi, H. Suda, *Bull. Chem. Soc. Jpn.* **1987**, *60*, 3659–3662.
[40] M. Newman, R. Kannan, *J. Org. Chem.* **1976**, *41*, 3–6.
[41] H. Staab, M. Zipplies, T. Müller, *Chem. Ber.* **1994**, *127*, 1667–1680.
[42] S. Elgafi, L. D. Field, B. A. Messerle, P. Turner, T. W. Hambley, *J. Organomet. Chem.* **1999**, *588*, 69–77.
[43] The amount of mono plus bis-ligand species is normalized to 100 %.
[44] Because of overlapping peaks it is not possible to integrate accurately at all temperatures and discuss this aspect in more detail.
[45] P. C. A. Bruijnincx, M. Lutz, J. P. den Breejen, A. L. Spek, G. van Koten, R. J. M. Klein Gebbink, *J. Biol. Inorg. Chem.* **2007**, *12*, 1181–1196.
[46] M. A. H. Moelands, PhD Thesis, Utrecht University, The Netherlands, **2014**.
[47] W. M. Haynes, *CRC Handbook of Chemistry and Physics*, CRC Press, **2015**.
[48] L. Pauling, *The Nature of the Chemical Bond*, Cornell University Press, **1960**.
[49] A. W. Addison, T. Nageswara Rao, J. Reedijk, J. van Rijn, G. C. Verschoor, *J. Chem. Soc., Dalton Trans.* **1984**, 1349–1356.
[50] Y. Uragami, T. Senda, K. Sugimoto, N. Sato, V. Nagarajan, E. Masai, M. Fukuda, Y. Mitsui, *J. Inorg. Biochem.* **2001**, *83*, 269–279.
[51] I. K. Valegård, A. C. van Scheltinga, M. D. Lloyd, T. Hara, S. Ramaswamy, A. Perrakis, A. Thompson, H. J. Lee, J. E. Baldwin, C. J. Schofield, J. Hajdu, I. Andersson, *Nature* **1998**, *391*, 806–811.
[52] A. L. Spek, *J. Appl. Crystallogr.* **2003**, *36*, 7–13.
[53] M. W. Vetting, D. A. D'Argenio, L. N. Ornston, D. H. Ohlendorf, *Biochemistry* **2000**, *39*, 7943–7955.
[54] T. Kurahashi, K. Oda, M. Sugimoto, T. Ogura, H. Fujii, *Inorg. Chem.* **2006**, *45*, 7709–7721.
[55] S. S. Rocks, W. W. Brennessel, T. E. Machonkin, P. L. Holland, *Inorg. Chim. Acta* **2009**, *362*, 1387–1390.
[56] G. Deacon, R. Phillips, *Coord. Chem. Rev.* **1980**, *33*, 227–250.
[57] E. G. Palacios, G. Juárez-López, A. J. Monhemius, *Hydrometallurgy* **2004**, *72*, 139–148.
[58] E. Pretsch, P. Bühlmann, M. Badertscher, *Structure Determination of Organic Compounds*, Springer, Berlin/Heidelberg, Germany, **2009**.
[59] Y. Feng, J. England, L. Que Jr., *ACS Catal.* **2011**, *1*, 1035–1042.
[60] K. Chen, M. Costas, J. Kim, A. K. Tipton, L. Que Jr., *J. Am. Chem. Soc.* **2002**, *124*, 3026–3035.
[61] K. S. Hagen, *Inorg. Chem.* **2000**, *39*, 5867–5869.
[62] G. R. Fulmer, A. J. M. Miller, N. H. Sherden, H. E. Gottlieb, A. Nudelman, B. M. Stoltz, J. E. Bercaw, K. I. Goldberg, *Organometallics* **2010**, *29*, 2176–2179.
[63] A. J. M. Duisenberg, L. M. J. Kroon-Batenburg, A. M. M. Schreurs, *J. Appl. Crystallogr.* **2003**, *36*, 220–229.
[64] G. M. Sheldrick, *SADABS*, University of Göttingen, Germany, **2008**.
[65] G. M. Sheldrick, *Acta Crystallogr., Sect. A Found.* **2008**, *64*, 112–122.
[66] G. M. Sheldrick, *Acta Crystallogr., Sect. C Struct. Chem.* **2015**, *71*, 3–8.
[67] A. L. Spek, *Acta Crystallogr., Sect. D Biol. Crystallogr.* **2009**, *65*, 148–155.
[68] Derived values do not contain the contribution of the disordered solvent molecules.
[69] A. M. M. Schreurs, X. Xian, L. M. J. Kroon-Batenburg, *J. Appl. Crystallogr.* **2010**, *43*, 70–82.
[70] A. L. Spek, *Acta Crystallogr., Sect. C Struct. Chem.* **2015**, *71*, 9–18.
[71] Bruker, *SAINT-Plus*, Bruker AXS Inc., Madison, Wisconsin, USA, **2001**.
[72] G. M. Sheldrick, *Acta Crystallogr., Sect. A Found. Adv.* **2015**, *71*, 3–8.

Received: December 3, 2015
Published Online: February 2, 2016

 